Test Results for Shaft Tracking Behavior of Pads in a Spherical Pivot Type Tilting Pad Journal Bearing

Giridhar Sabnavis

Thesis submitted to the faculty of the Virginia Polytechnic Institute and State University in partial fulfillment of the requirements for the degree of

Master of Science
in
Mechanical Engineering

Dr. Gordon Kirk
Academic Advisor
Committee Chair

Dr. Mary Kasarda
Committee member

Dr. Zenglin Guo
Committee member

14th April 2005
Blacksburg, VA

Key words: Spherical pivot bearings, pad motion, pivot friction, shaft tracking

Test Results for Shaft Tracking Behavior of Pads in a Spherical Pivot Type Tilting Pad Journal Bearing

Giridhar Sabnavis

(Abstract)

Most tilting pad journal bearing dynamic characteristics estimation methodologies assume perfect shaft tracking by the pads. In other words, they neglect pivot friction. In case of pads having point or line contact that operate under most normal load conditions, the pad tilting is due to a rocking motion which is not greatly influenced by friction. Hence this simplifying assumption might be acceptable. Heavier loading conditions, such as those typically encountered in gearboxes, demand the use of spherical pivots to avoid pivot failure. The spherical pivot is very attractive for this reason, but the tilting motion is rather a sliding action that must occur in the precision ball socket. A valid concern exists for verifying the soundness of assumed shaft tracking by the pads of such bearings. A "fixed test bearing, floating shaft" type of test rig previously built for determining the dynamic characteristics of bearings was accordingly modified to facilitate the testing of shaft tracking for a spherical pivot bearing.

This thesis describes the modifications carried out on the rig. The special instrumentation and data acquisition systems implemented to observe the minute pad motion are also discussed. Some preliminary results of the tests are presented for various loading conditions. They show excellent shaft tracking by the pads. More detailed testing and analysis of data is required to fully understand the pad motion and tracking ability of the spherical pivot design.

Key words: Spherical pivot bearings, pad motion, pivot friction, shaft tracking

Acknowledgments

I take this opportunity to express my heartfelt gratitude towards my academic advisor, Dr. Gordon Kirk. You have taught me something more precious besides the wonderful science of rotordynamics. Your patience, equanimity and professionalism are traits I will forever cherish and try to emulate. I hope I will be a good rotordynamicist, but more importantly, I want to be a better person, more reliable and understanding. Thank you Dr. Kirk for instilling this desire in me.

I thank Dr. Kasarda and Dr. Guo for agreeing to serve on my committee.

I thank my parents and my brothers for all the support and succor they gave me. I drew a lot of strength and confidence from the fact that you all stand by me. I hope I can live up to your expectations now and for ever.

I thank my lab mates Andy, Jess, Kenan, Ali and Dr. Guo for the wonderful company, simulating discussions and invaluable help on my experiment. Things would have been so much more difficult but for you people.

I thank my friends Aroon, Kavita, Vikram and Wilfred for being with me through thick and thin. You have made my graduate life a whole lot different, more pleasant and fun. You were my family away from family and put up with my moods and made my good times better. Thanks for everything.

I would finally like to thank Dr. Nicholas and others working at RMT for the timely delivery of the test bearing and for patiently answering my numerous questions.

Table of Contents

List of figures

List of tables

Nomenclature

c	=	Assembled bearing radial clearance
t	=	Time from keyphasor blip to the nearest successive positive peak
D	=	Bearing diameter
L	=	Pad length
M	=	Magnitude of load exerted by magnet assembly on rotor
N	=	Rotor speed
R	=	Bearing radius
So	=	Dimensionless Sommerfeld number
T	=	Time period of synchronous vibration signal
W	=	Load on bearing
μ	=	Viscosity of oil
Φ	=	Phase angle of synchronous vibrations

Chapter 1

Introduction

This thesis presents the work carried out towards conducting some unique and never before attempted experimental studies on pad motion in a spherical pivot type tilting pad journal bearing. Over the next five chapters, the motivation behind the study, a description of the equipment used, the test procedure adopted and the data obtained are presented. Preliminary conclusions based on the analysis of the obtained results are drawn after a basis for correlation is made. Finally, recommendations for further study and future research in this interesting area are made.

1.1 Background

The rotor assembly is the most critical component in high performance rotating machines like turbines, expanders, pumps, compressors and generators. Rotors of such machines have several important dynamic attributes which might adversely affect the overall reliability of the machine. These attributes include response to unbalance, susceptibility to rotordynamic instability due to various factors and acceptable startup and shutdown capabilities. These are a manifestation of the complicated interaction between the working fluid, the rotor, the bearings and seals and the support structure. The designer needs to understand each component of the complex system to be able to understand the overall behavior of the rotor system. Bearings are probably the most important elements in the rotor-support system as they can significantly affect its overall damping and stiffness.

Fluid film journal bearings (FFJB) are widely used to support the rotor in the casings or on the pedestals of these machines. In comparison with rolling contact bearings, well designed FFJBs have several desirable features such as low to moderate cost, near infinite service life and moderate to very good vibration damping characteristics, amongst others. Many different types of FFJBs have been developed to cater to the diverse operating needs of modern rotating machines.

In the increasing order of their sophistication and manufacturing cost, different bearing types can be arranged as follows:

1. Plain cylindrical
2. Two lobe/two axial groove
3. Offset half
4. Thee/Multi lobe
5. Pressure dam
6. Tilting pad

It can thus be seen that the bearing designer is faced with a wide variety of choices for a given application and has to base his decision on proven analysis and evaluation methodologies. Researchers have worked tirelessly to develop sophisticated techniques to analyze bearings. The most important aspect of design and analysis of bearings is the ability to accurately predict their dynamic characteristics and other properties such as oil flow, horsepower loss and film temperature. In cases where tilting pad bearings are employed, there are additional and seldom overlooked phenomena like pad flutter and pivot stresses that also need to be accounted for. Several techniques have been developed to analyze bearings and are extensively used by the industry. Most are analytical or numerical methods validated in some cases by comparison to experimentally observed values.

1.2 Tilting pad bearings

FFJBs can be broadly classified into two categories, fixed geometry and tilting pad type. Tilting pad bearings (TPB) are rapidly becoming the bearings of choice for small and medium sized rotors operating at medium to high speeds. They have several distinct advantages over fixed geometry bearings that make them specially suited to light load operation. Primary amongst them is the near total absence of self excited instabilities called *'oil whirl'*. They suffer from certain drawbacks, such as higher manufacturing cost, lower load carrying capacity and higher parasitic losses compared to fixed geometry bearings of similar dimensions. But in most cases, the advantages far outweigh the drawbacks and they continue to find a wide application in the turbomachinery industry.

Tilting pad bearings consist of several arc shaped segments called 'pads' that are assembled into a circular housing forming a bore. The pads rest on pivots and are free to

rock or slide on them to achieve the tilting motion. The journal is accommodated in the bore with a clearance around it. Under dynamic motion of the shaft center, the pads tilt and re-orient themselves such that the load vector always passes through the pivot point. Due to this, the destabilizing '*cross-coupling*' forces in the bearing are eliminated and they are free from self induced instabilities like '*oil whirl*'.

Tilting pad bearings can be classified into the following categories based on the type of pivots they employ:

1) Point contact (Sphere in cylinder)
2) Line contact (Rocker back or axial pin type of pivot)
3) Surface contact (Ball in Sphere)

It may be noted that they are arranged in the increasing order of load carrying capacity based on pivot strength. Several techniques have been developed to increase the load carrying capacity of TPBs by keeping bearing metal temperatures low and by preventing pivot failure under heavy loading. For completeness, they are described below.

There has been a continuous trend to increase the load carrying capacity of tilting pad journal bearings. Increased capacity results in smaller bearings for a given application or in larger and heavier rotors for the same bearing size. This has a downstream effect of reducing the bearing parasitic losses and the size of the lubricating oil system and overall reduced capital and operating costs. Two distinct factors limit the load carrying capacity of a tilting pad bearing, viz. the maximum pad metal/oil film temperature and the pivot stresses.

(i) Oil film/pad metal temperature: High loads and high surface speeds result in high oil film temperature which can lead to premature failure of pads and deterioration of oil. Researchers have experimented with several methods to reduce the maximum oil temperature. These include using offset pivots, directed lubrication and application of high thermal conductivity material like copper as pad base. Nicholas [4] used these traditional methods and also some innovative techniques like hot oil carryover reduction and bypass cooling to achieve never before achieved load carrying capacities in tilting pad journal bearings for gearbox applications. He achieved 470 *psi* of loading at a surface speed of 420 *ft/sec* in a 6 *inch* bearing, the traditional limits being 200 *psi* at 300 *ft/sec*.

(ii) Pads transfer the dynamic and the static loads acting on them to the machine structure through the pivots, hence pivots are the most stressed components in bearings. They undergo deformation, both elastic and plastic due to these stresses. Kirk and Reedy [2] emphasize the importance of including the pivot deformation and stiffness while calculating the stiffness and damping properties of tilting pad bearings. The overall dynamic properties of a bearing can be significantly reduced when low stiffness pivot configurations are used. They discuss methods to evaluate the stiffness of three popular pivot types, (i) cylindrical pivots in cylindrical housings (line contact), (ii) spherical pivots in cylindrical housings (point contact) and finally, (iii) sphere in sphere type of pivots (surface contact, the type used in the current experiment). Knowing the pivot type, load on the pad and material properties, it is possible to calculate the stiffness of the pivot using simple formula. The stiffness and damping of the oil film for each pad can be calculated using established finite difference or other methods to solve the governing equations. The equivalent stiffness and damping of each pad/pivot combination can then be calculated and these values can be used in a pad assembly type of program to calculate the dynamic properties of the complete bearing. They go on to show that the sphere in sphere configuration has the highest stiffness when the difference in the pivot and the cavity diameters is less than 1%. Nicholas [3] too talks about pivot stresses and resulting effects. He shows examples of poorly designed pivots that failed in service due to high Hertzian stresses.

Returning to the subject of analysis of TPBs after the brief digression, It is known that due to their additional degrees of freedom, the analysis of tilting pad bearings is more involved than fixed geometry bearings. Nicholas [6] summarizes some of the classical techniques of analyzing tilting pad bearings. He talks about the modest beginning in the 1950`s when the TPBs were approximated to tilted pads against flat runners to the more advanced ones today that include pad inertia, pad deformation due to thermal and elastic effects, pivot deformation and film turbulence. In spite of the great advances made in both the analysis methods and the hardware on which these complicated calculations are carried out, most techniques still make the following assumptions:

1) The pads vibrate with the same frequency as the rotor, and
2) Friction between the pad and the pivot is negligible.

These assumptions have a very great simplifying effect on the calculations while supposedly having only a marginal effect on their accuracy. This has never been verified, least of all experimentally. The validity of these assumptions is particularly questionable in case of spherical pivot bearings where pivot friction could become much larger than in a rocking pivot bearing. The present study is aimed at experimentally verifying these assumptions in a spherically pivoted bearing under different conditions of load, speed and unbalance.

1.3 Spherical pivot bearings

Spherical pivot bearings (SPB) consist of the usual pads and several pivots that are made of hardened steel. These pivots are hemispherical in shape and are attached to the bearing housing at fixed angular locations. Each pad has a precision machined cavity on the underside and the pivot goes into this cavity when the bearing is assembled. *Figure 1.1* below shows a spherical pivot bearing. Because of greater contact surface, the Hertzian stresses are lower at the pivot and as a reason the load carrying capacity of these bearings is higher than other kinds of tilting pad bearings. The increase in the contact surface has another consequence in that the mechanism of pad tilt changes from rocking to sliding. This introduces a new factor, *viz.* pivot friction that must be accounted in the analysis. Excessive friction impedes pad motion and there could be a reduction in shaft tracking behaviour of the pads.

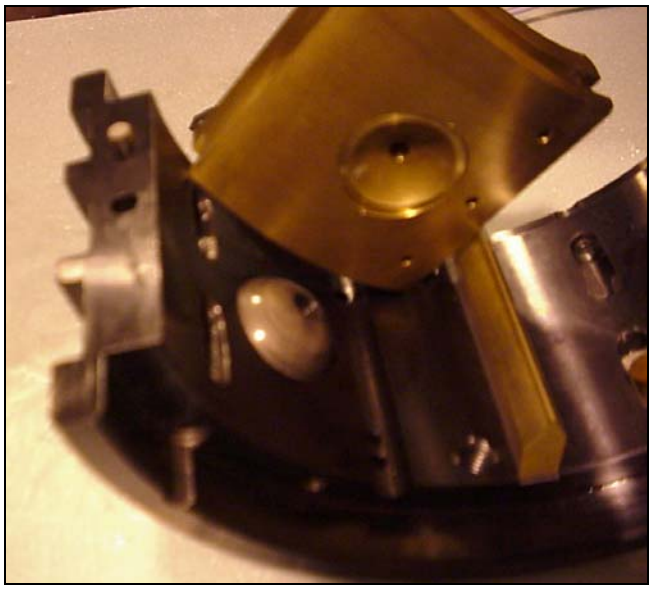

Fig 1.1 Spherical pivot bearing

1.4 Thesis outline

The FFJB test rig used for the current experiment is briefly described in the next chapter along with some studies previously conducted on it. The subsequent chapter describes several important modifications carried out on the existing rig in order to conduct the present study. Chapter 4 talks about the theoretical aspects of pad motion. Some experimental studies conducted by other researchers with regard to pad motion and its effects on bearing properties are reviewed. The chapter closes with a description of the procedure developed for the present experiment. The test cases and obtained results are presented in Chapter 5. A basis for comparing shaft and pad motion is also evolved; this is followed by a brief discussion of the results. The thesis ends with a summary of the test results and the conclusions drawn thereof. There is immense scope for further experimentation and analysis in this area and some recommendations for future work are made in the last chapter.

Chapter 2

VT FFJB Test Rig

2.1 Introduction

The Virginia Tech Fluid film journal bearing (VT FFJB) test rig used in the present study is briefly described in this chapter. The rig is described in greater detail in several earlier works by Swanson [11, 12].

The test rig is a unique "floating shaft, fixed test bearing" type. It is one of the few rigs of its kind. The other kind, namely, the "fixed shaft, floating test bearing" is more popular among researchers. Easier installation, straight forward controls and simpler instrumentation are some reasons for its more widespread usage. The factor in favor of the current setup is that it better mimics the arrangement in most real world machines where the bearings are indeed fixed (to the casing/pedestals) and the rotor is floating.

The current test rig has several features that make it attractive for the present experiments, while several other features had to be modified from previous tests carried out on it. The test bearing fits into a cavity in the front of the rig, the bearing is supported on four load cells, two on each side, arranged at ± 135° from the vertical centerline. The load on the bearing could be reckoned from the readings of the four load cells. But due to their limited accuracy and excessive drift, their readings are seldom reliable and hence were almost never used. Instead, the load cells under the electromagnets (described in the next section) were used to measure the load exerted on the shaft and thereby the bearing. Tapped equi-spaced holes are available on the test bearing end of the rotor to add unbalance weights. To begin with, the rotor is assumed to be well balanced; this is borne out by the very low synchronous vibrations observed in the entire range of test speeds.

2.2 Design and key features

The rig consists of the following systems whose functions are briefly described alongside:

Drive: The test rig rotor is driven by an AC Induction motor via a speed increasing pulley-belt arrangement. The motor speed can be controlled quite accurately by means of a computer controlled VFD system. The present setup allows the rotor to reach speeds of up to 10,000 rpm but, due to excessive noise due to belt flap and structural vibration of the motor mount, the top speed for the present study was limited to 7000 rpm.

Lube oil system: A complete LO system consisting of an adequately sized tank, pump, filter, oil cooler, flow and pressure gages and drain return pipe is available to supply required amounts of lubricating oil (Exxon Teresstic GTC 32/ISO VG-32) at desired pressure to the bearing. Certain key modifications were carried out on the LO system to improve its' functionality and they are described in a later chapter.

Shaft alignment system: The test rig is equipped with an automatic shaft alignment system to correct any changes in the state of alignment due to thermal growth of supports or bending of the shaft. The test bearing is fixed to the structure while the rear ball bearing can be moved horizontally and vertically to ensure that the bearing axis and the shaft axis maintain the desired relative disposition. The shaft alignment was not observed to change significantly during the present study, primarily due to the short periods of operation (~5 minutes per test case). Hence the alignment system was seldom used during the present study.

Magnetic loading system: The test rig is equipped with a sophisticated magnetic shaft loading system with automatic controls. Three electromagnetic segments are arranged around the shaft with an air gap. Force exerted by each individual magnet can be controlled to achieve any desired magnitude (up to a maximum) of steady or varying force in any direction. Current is fed to the electromagnets from a bank of PWM amplifiers. The amplifiers are in turn controlled by a control card which performs the mathematical optimization and decides the value of the current to each segment so as to

achieve a desired load set point. Saturation of the electromagnets occurs when the shared load between any two segments is approximately 6672 N (1500 lbs). Since the magnets are arranged at ± 60° and 180° from the TDC, this is possible only at angles of 0° and ± 120° from the TDC. *Figure 2.1* below shows the arrangement of the magnets and the positions of maximum applied load. This system was extensively used to study behaviour of the bearing for various steady loads.

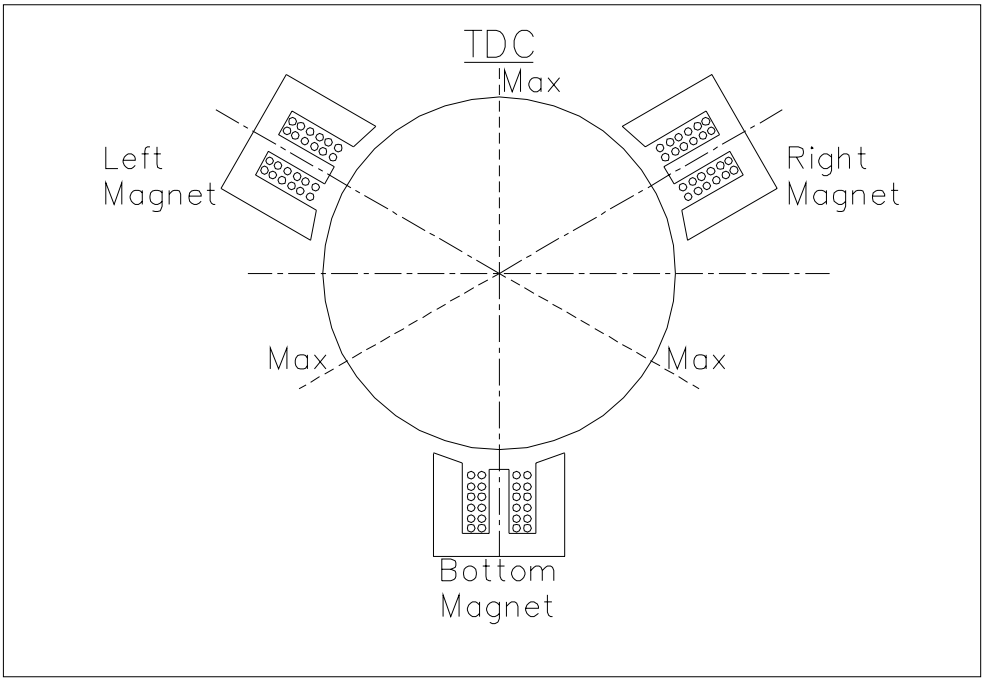

Fig 2.1 Arrangement of electromagnets

Rotor-bearing system: The 990.6 mm (39") long forged steel rotor is supported on a double ball bearing (rear bearing) on the right side and the test bearing on the left. A flexible, multi-membrane coupling connects the ball bearing end of the rotor to a stub shaft. The stub shaft is connected to a pulley which is connected to the motor shaft by means of a 'poly-vee' belt. The weight of the rotor, together with the half-coupling, rotor laminations and lock nuts is 58 kg (128 lbs) of which 34 kg (75 lbs) is supported by the test bearing. The test bearing transmits loads to the rig structure through a bank of load cells. But due to excessive drift and poor precision, they were not used for measurement. Instead the load cells under the magnets were used to reckon the load on the bearing. The test bearing end of the rotor has tapped holes for introducing unbalances, these were used to conduct tests at different levels of unbalance. *Figure 2.2* shows a schematic of the rotor; some key dimensions are also shown. All dimensions are in *mm* (*inches*).

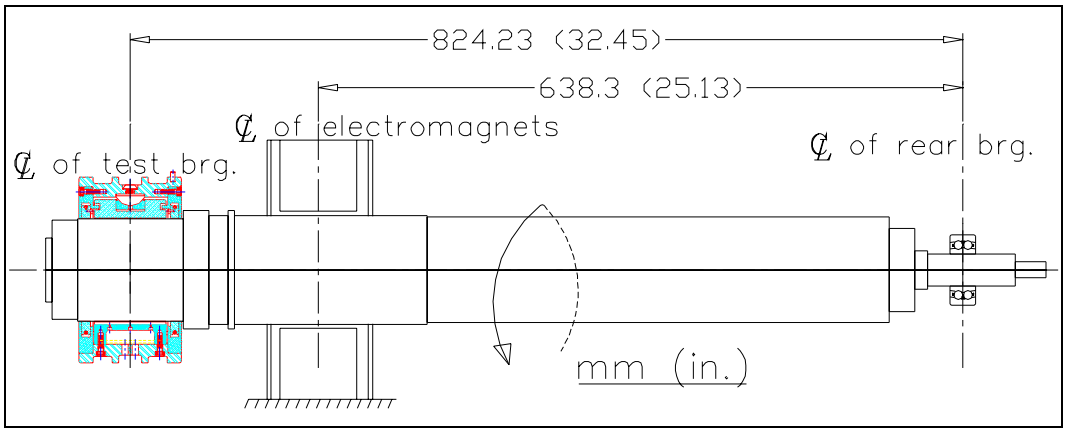

Fig 2.2 Schematic of test rig rotor

Figure 2.3 shows a sketch of the bearing used in the present experiment. The right side cover and floating oil seal have not been shown for clarity. Provision was made for mounting eight pad motion probes, but only four were actually used as explained in a later section. Some important dimensions and details of the bearing are given in Table 2.1 below.

Table 2.1 Bearing details

Parameter	**Value**
Number of pads	4
Nominal Orientation	Load between pads
Angular location of pivots w.r.t the TDC	45°, 135°, 225°, 315°
Pivot offset	50%
Pad angle	71°
Set bore diameter	101.8032 mm (4.008 in.)
Pad length	71.12 mm (2.8 in.)
Bearing length	101.6 mm (4.000 in.)
Journal diameter	101.575 mm (3.999 in.)
Preload	0.5
Bore Clearance	203 μm (8 mils)
Pad Clearance	406 μm (16 mils)
Pivot diameter	31.750 mm (1.25 in.)
Socket diameter	31.763 mm (1.2505 in.)

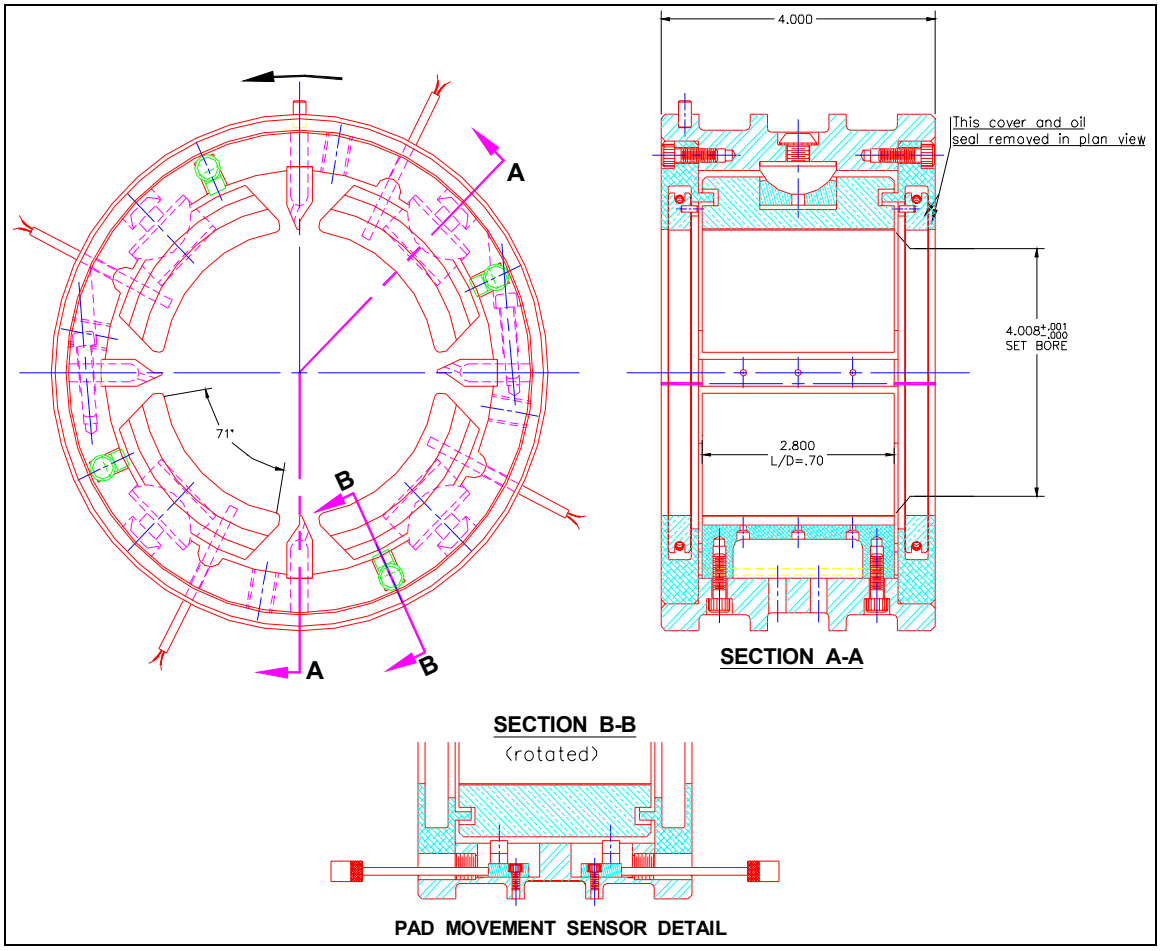

Fig 2.3 Sketch of test bearing

Data acquisition: The test rig has fully automatic data acquisition capabilities. All important dynamic data such as rotor speed, shaft and pad vibration, oil inlet and bearing metal temperatures etc. are automatically collected. Only relevant data, like speed and vibration, are stored for retrieval, the rest are displayed in real time and not stored. Static data like oil feed pressure and flow are displayed in real time and are manually recorded. Sufficient care was taken to ensure that the various parameters do no fluctuate during a test run.

Several important modifications were carried out on the data acquisition system and they are described in detail in the next chapter. The pad and shaft motion monitoring instruments are also described in the next chapter.

2.3 Previous studies conducted on VT FFJB test rig

The VT FFJB has been previously used for several important studies on bearings. They are listed chronologically below to gain an appreciation of the features and capabilities of the current test rig.

Swanson and Kirk [10] present the problems they encountered when designing the current rig and running the first set of experiments on it. They observed unexpected phase shifts in measured shaft response data. This led them to conducting experimental modal investigations of the shaft dynamics. Both traditional impact and scanning Doppler laser velocimeter techniques were used to develop a tuned rotor dynamic model which was subsequently used to help understand and explain the unexpected phase shift observations. It was discovered that the rig could not be used to carry out dynamic tests without making extensive modifications. The results from this analytical study highlight several design issues which should be considered by future test rig designers to avoid similar difficulties.

Examination and comparison of the maximum film temperature in a journal bearing for 13 synthetic, mineral, and viscosity index enhanced oils was carried out by Swanson et al. [8] using the present rig. This study examined the differences between the various oils with regards to peak oil film temperatures. Data for each type of oil was obtained at various speeds ranging from 6000 rpm to 14000 rpm and for loads ranging from 670 N to 3400 N. A 50.8 mm diameter, 25.4 mm long bearing with the upper portion relieved was used for all tests.

Swanson and Kirk [7] examine the experimental temperature and pressure profiles for a steel and a bronze bearing using the test rig. A potentially powerful effect on the characteristics of plain journal bearings is local thermal deformation of the bearing surface. Although there are a few analyses that consider the effect, it is ignored by most journal bearing codes used by industry. There is also almost no experimental data in the literature that focuses on this effect. To generate such data, two identical (101 mm x 57 mm) bearings, one fabricated from steel and one from bronze have been tested in a precision journal bearing test rig. Comparisons between shaft displacement data for steady loading of the two bearings show that the deformations are important to consider.

Chapter 3

Modifications carried out on FFJB test rig

This chapter describes the various modifications carried out on the existing FFJB test rig to make it suitable for the present experiment. The rig and its' features, systems and capabilities are discussed in detail in Swanson [11, 12]. For completeness, they were also briefly described in Chapter 2 of this thesis.

3.1 Lubricating oil system

The first system that received attention was the existing lubricating oil (LO) system. It consisted of a Stainless steel tank (20 gal capacity) and a motor driven sliding vane pump that delivered oil to the bearing. The oil was routed through a filter (15 microns, paper element) and a shell and tube type heat exchanger upstream of the bearing. Oil pressure and flow could be controlled by means of a bypass valve. The temperature of the oil could be controlled quite accurately using a 1000 kW electrical tank heater and the water cooled heat exchanger. The temperature control function is automated by using a Yokogawa UT-351 process controller. Any desired set temperature can be reached and held constant by the controller.

The existing tank was too small for a system that needed a continuous supply of oil at the rate of 4~8 gpm. Due to the low reservoir capacity, sufficient residence time was not available for the air dissolved in the oil due to cavitation in the bearing to escape. Excessive air entrainment in the oil resulted in extensive foaming. This made the oil very bubbly and as a result it was almost impossible to accurately estimate the viscosity of the oil. Hence it was felt that a larger tank with greater surface area was needed. A tank (42"x48"x15") was fabricated out of SS sheet. The capacity of this larger tank is 100 gal. Oil from the old tank was drained and piping was disconnected. The new tank was installed on a wooden frame set on the concrete floor. All piping and instruments (oil

level and temperature) were hooked up. The heater was connected to the appropriate power supply and inserted in the tank. *Figure 3.1* shows the new tank after installation. A fume/dissolved air extraction fan was also installed to evacuate the tank of air. This further helped mitigate the 'bubbly oil' problem. It can be seen on the far right hand corner of the figure. A new filter and rerouted gravity drain system were also installed.

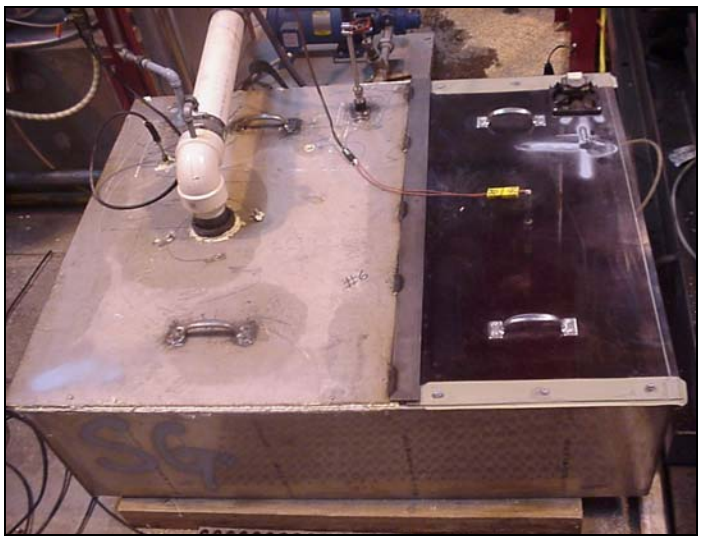

Fig 3.1 New oil tank after installation

3.2 Instrumentation

Selecting the right instrumentation for observing pad motion presented one of the greatest challenges. Several factors had to be considered before deciding on what instruments to go with. Due to the severe space constraints, the probes had to be as small as possible and due to the extremely small range of motion expected at the pads, the probes had to be sensitive enough and fairly linear in the range of expected motion. Finally it was decided that eddy current type proximity probes were the best suited for this application. Probes supplied by several manufacturers were examined and it was decided that a specially developed 90° bent probe by Bently Nevada (not introduced in the market yet) is right for the application. *Figure 3.3* shows a close up of the probe. A manufacturer supplied sketch, shown in *Fig 3.2* gives detailed dimensions of the probe.

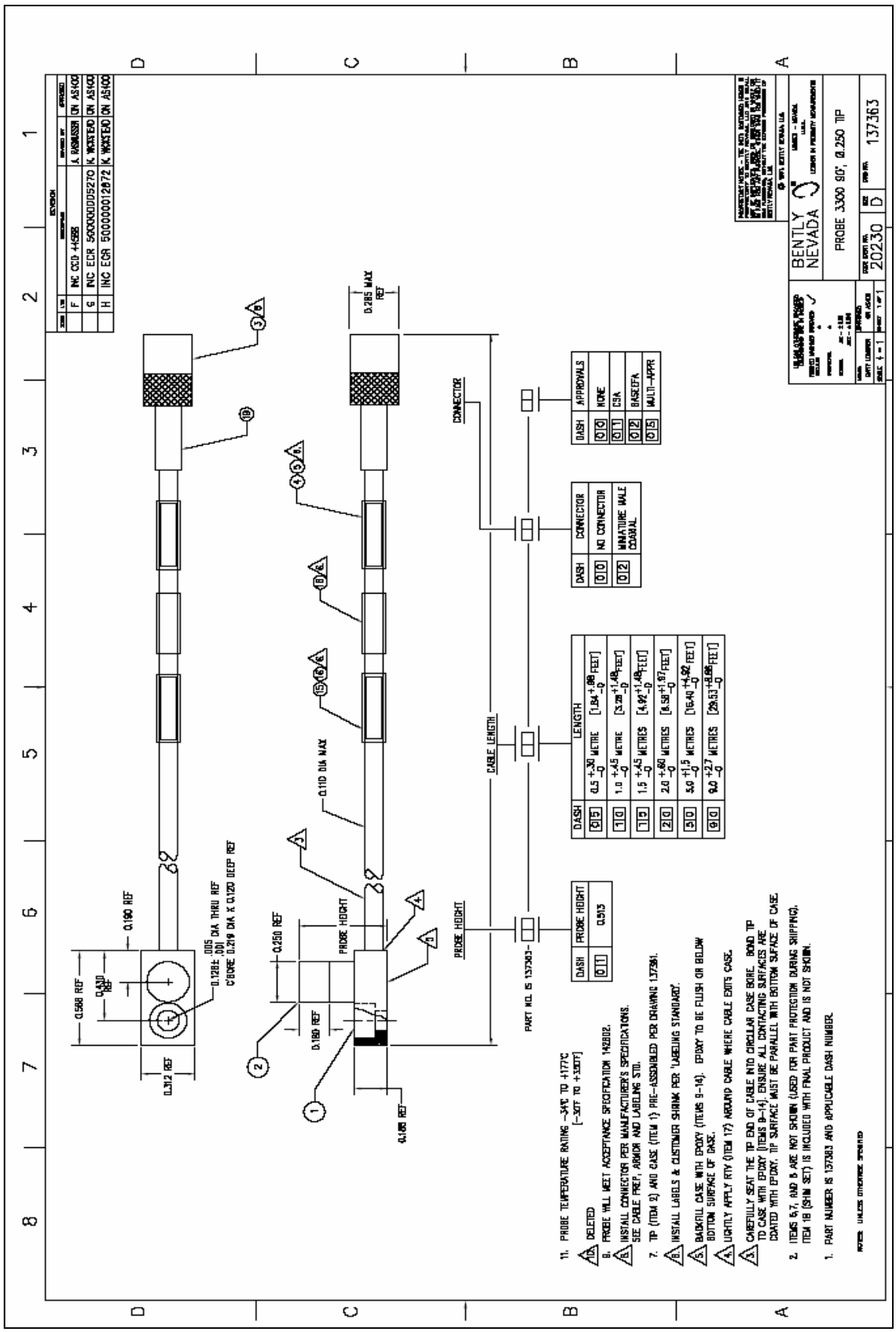

Fig 3.2 Manufacture's sketch of pad probe

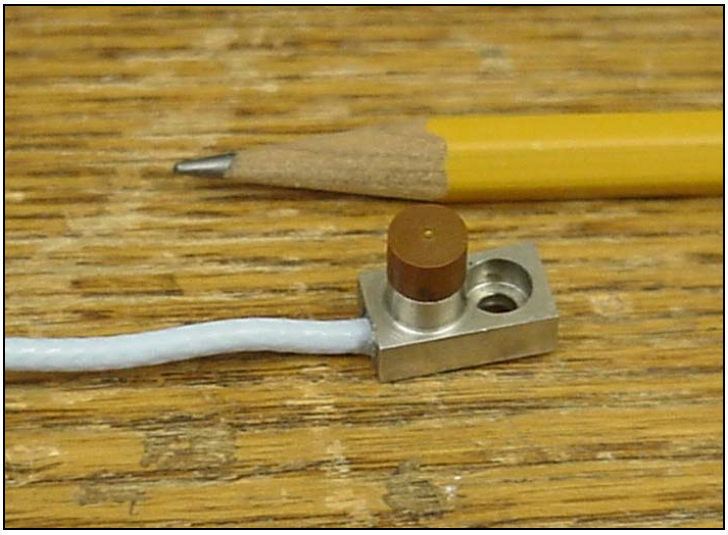

Fig 3.3 Close up of pad motion probe

The following figure (*Fig 3.4*) shows the placement of the probe in the bearing so as to observe the pad motion where it is at a maximum for a given tilt subject to space and assembly constraints. The pad probes are at an angle of 15° (~57% from pivot) from the leading edge of the corresponding pad. Also see *Fig 4.8* for a better understanding of the arrangement of pad and shaft probes.

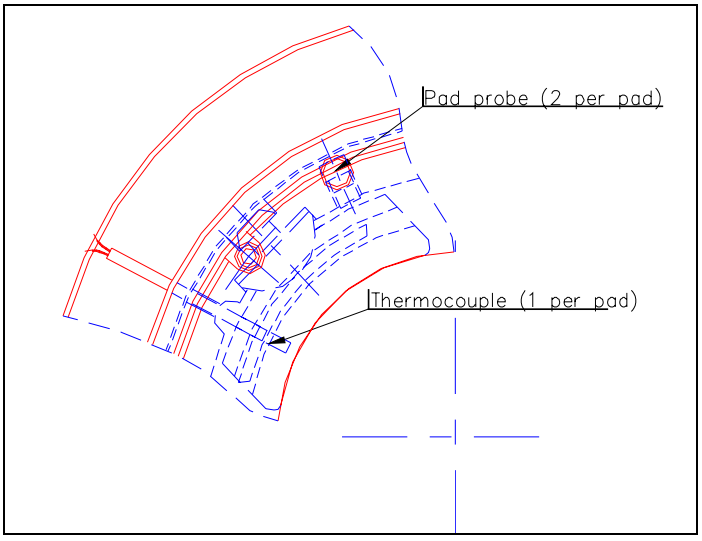

Fig 3.4 Arrangement of pad instruments

Two probes, one on the inboard side and the other on the outboard side were installed on each of the top two pads. It was decided to leave the bottom half of the bearing un-instrumented due to severe space and assembly constraints.

With the help of the magnetic loading system present in the rig, any kind of loading situation could easily be simulated. Thus the un-instrumented half is not expected to seriously affect the experiment. The probe was calibrated with a bronze target (pad material) and *Fig 3.5* below shows the calibration curve. Based on the curve, the linearity range is clearly between 127 μm (5 mils) to 1651 μm (65 mils) and the sensitivity is approximately 12.6 mV/μm (320 mV/mil).

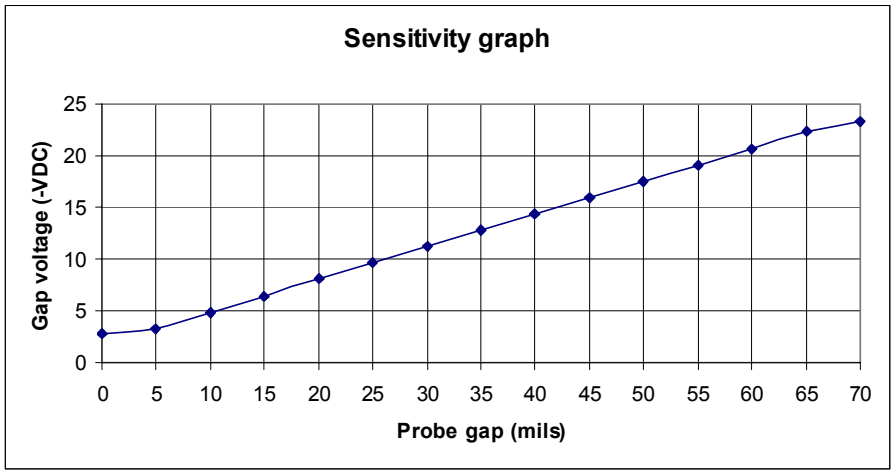

Fig 3.5 Calibration curve for pad probe on Bronze target

To check the correctness of the method used to calibrate the probe, the method was used to calibrate the probe for a 4340 steel target. The sensitivity was found to be 7.87 V/mm (201 mV/mil) which is the exact value specified by the manufacturer. The calibration curve of the probe for 4340 steel is shown in *Fig 3.6* below.

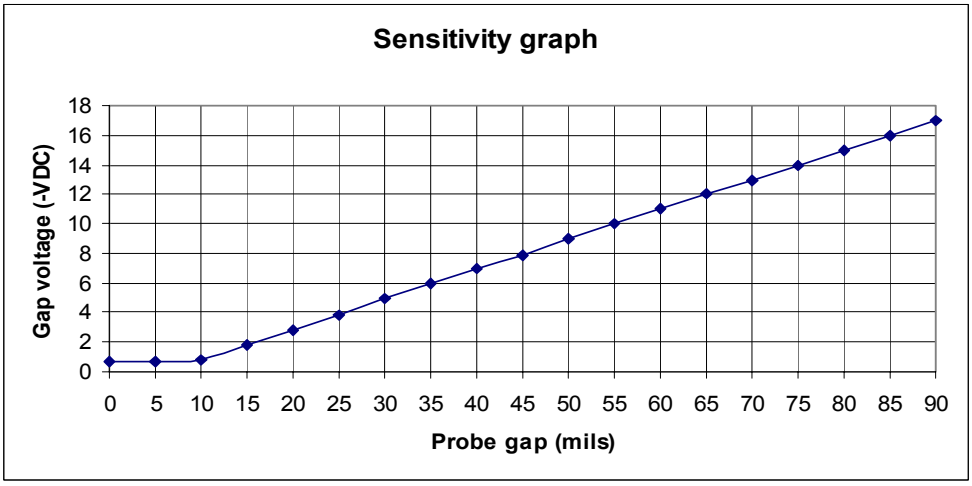

Fig 3.6 Calibration curve for pad probe on 4340 target

Two orthogonal shaft vibration probes were installed on each side of the bearing (inboard and outboard). The shaft proximity probes (8mm, BN type) were accurately lined up with the pad probes, this had the advantage that now the pad probe response could directly be compared with the response of the corresponding shaft probe without any rotation or transformation of axes, while the disadvantage is that the probes are now located at a rather unusual angle of +25° and -65° from the TDC. This caused some problems with some auxiliary functions like the automatic alignment of the rotor and temperature compensation of the shaft probes. For reasons mentioned in Chapter 2, these functions were seldom used and hence the experiment was not adversely affected in any manner. *Figure 3.7* below shows the arrangement of one pair of shaft and pad probes. The pad probe has been rotated from position by 180° for clarity.

A probe tip clearance of 890 μm ~ 1016 μm (35 ~ 40 mils) was maintained for the pad probes while it was held at 635 μm ~ 890 μm (25 ~ 35 mils) for the shaft probes. In addition to pad motion probes, 'J' type thermocouples were inserted (one per each pad) in the 75%-50% position to monitor pad temperature. Flexible leads with generous kinks were selected so as to have the least influence on the pad motion.

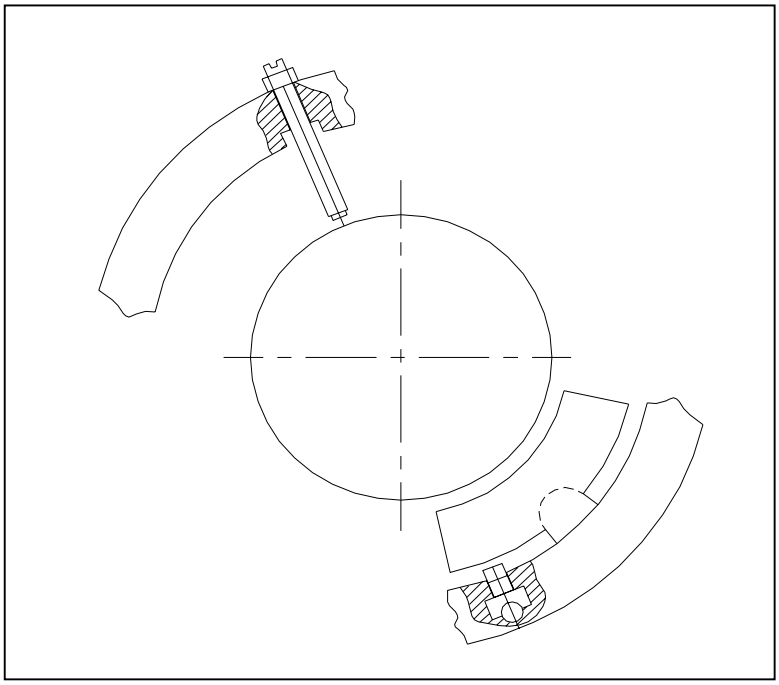

Fig 3.7 Arrangement of shaft and pad probes

3.3 Data Acquisition

The existing automatic data acquisition system was used for static data like the load exerted by the magnetic system, oil pressure and temperature etc. For vibration and shaft motion data acquisition, ADRE 5.1 together with a 208-P Data Acquisition Interface Unit from BNC was chosen. The software has excellent compatibility with the transducers used and has several data presentation formats which are of direct relevance to a rotordynamicist and thus eliminates laborious customization needed with general purpose data acquisition systems like LabView®. The 208-P DAIU is an 8-channel interface unit and hooks up directly with most commonly used vibration monitoring instruments. It connects directly to an EPP enabled port on a computer and the four pad probes and corresponding four shaft probes were connected to it as per the following table.

Table 3.1 Channel names and numbering scheme

Channel #	Channel name	Comments
1	Right Pad inside	
2	Top Pad inside	
3	Right Pad outside	
4	Top Pad outside	
5	Right shaft inside	Channel pair
6	Top shaft inside	
7	Right shaft outside	Channel pair
8	Top shaft outside	

From the wide variety of data presentation formats available, it was decided that the following ones were most relevant for the present study:

1. 1x Time trace, showing the amplitude and keyphasor mark both shaft and pad
2. 'Half' spectrum showing various components in the vibration both shaft and probe
3. Direct Time trend plot comparison showing one pad and corresponding shaft vibration

Analog oscilloscopes were also used to observe shaft orbits and pad motion in real time and study the influence of noise on the signal. In addition, oil temperature and flow rate were recorded manually from the indicating instruments for each test case. No real time temperature and flow data was stored as it was not considered to be relevant for this study.

Chapter 4

Pad motion studies

This section talks about the various aspects of pad motion and their influence on the overall characteristics of the bearing. Past work conducted by researchers in this area is reviewed. The chapter concludes with the presentation of the strategy adopted for the current experiment.

4.1 Factors affecting pad motion

Figure 4.1 shows a simplified model of a pad in a spherical pivot bearing. Only one pad is shown for simplicity. Various factors affecting shaft motion are shown, albeit in a simplified and lumped form. The oil film, the pivot and the friction at the pivot/pad interface can each be represented by a combination of a spring and a damper. The individual elements are non-linear in nature, but can be assumed to be linear, at least in the narrow range of the normal operation of the bearing.

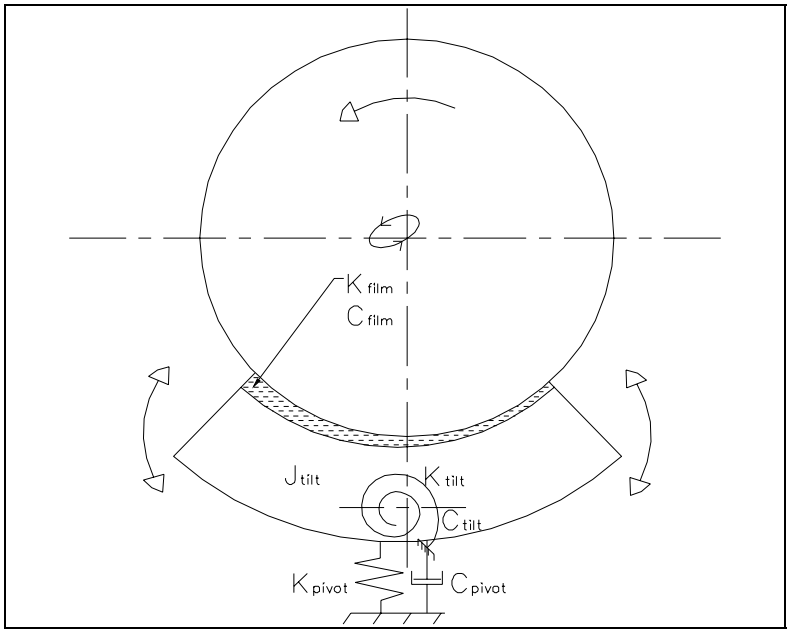

Fig 4.1 Model of pad in a SPB

In the figure,

K_{tilt} = Resistance to tilting motion of the pad (due to friction at pivot)

C_{tilt} = Damping to pad motion

K_{pivot} = Pivot stiffness

K_{film} = Stiffness of the oil film

C_{film} = Damping of the oil film

C_{pivot} = Pivot damping

J_{pad} = M.I of the pad about the axis of tilting

Most tilting pad analysis codes assume the following:

K_{tilt}, C_{tilt} = 0 (no friction at pivot)

K_{pivot} = Very high (near infinite pivot stiffness)

C_{pivot} = 0 (no damping at pivot)

K_{film} = Stiffness of the oil film as obtained from governing equation

C_{film} = Damping of the oil film as obtained from governing equation

J_{pad} = 0 (Neglect pad rotational inertia)

Because of these assumptions, the pad has a pure tilting motion (no rectilinear motion) and tracks the shaft motion perfectly. But in reality K_{tilt}, C_{tilt} and J_{tilt} are all non-zero values; this introduces a phase difference between the shaft and the pad motions. The following lumped model shown in *Fig 4.2* is a better representation of the shaft-pad-pivot system than the over-simplified and commonly used lumped mass-spring-dashpot model. More research is needed to find suitable mathematical models to represent the newly introduced quantities like K_{tilt} and C_{tilt} that could be strongly non-linear.

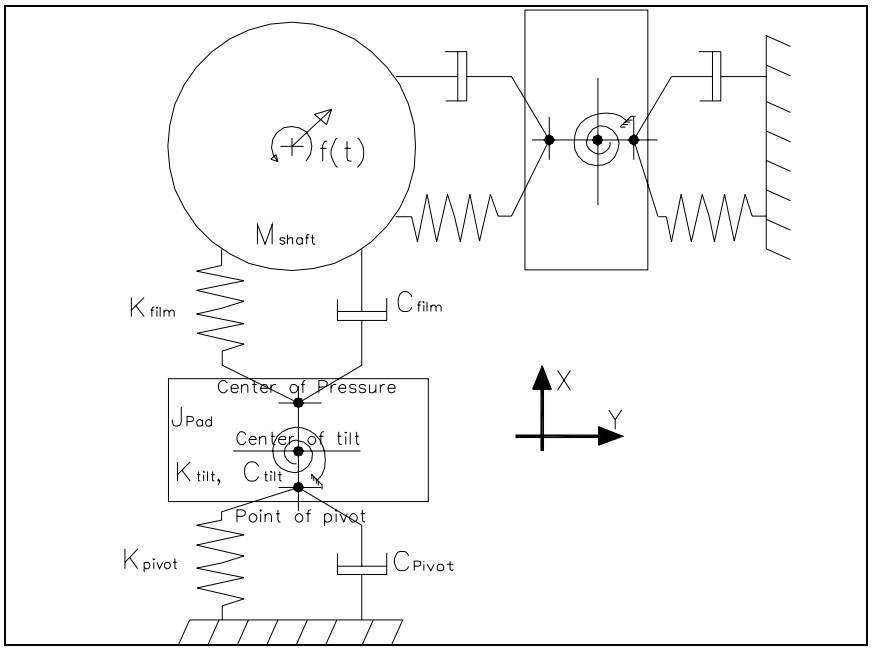

Fig 4.2 Improved model of a SPB

4.2 Literature survey

Papers that discuss the two previously mentioned and hitherto unverified assumptions are reviewed in this section. Papers addressing the different pivot types commonly used in FFJBs are also discussed. They were the starting point for this experiment and much of the present study is built around the issues raised in these works.

Nicholas [6] presents an excellent review of Lund's landmark paper on the pad assembly method. Subsequent works by other researchers that either improved on Lund's method or were based on it are also covered. He discusses the far reaching rotordynamic implications of Lund's method. Lund was the first to assume synchronous frequency of pad vibration and he gives four stiffness and four damping curves for tilting pad bearings he analyzed. He also mentions that when the pad inertia is neglected, the cross coupled terms vanish and the characteristics are further reduced. This is the common assumption of bearing analysis codes used by a majority of the industry. The rationale behind assuming synchronous pad frequency remains a subject of debate. When reduced bearing coefficients were used for stability study, Lund himself pointed out that the method is flawed and mathematically incorrect. Nevertheless, the use of synchronous coefficients for forced response and stability calculations is a valid assumption for machines with dominant synchronous content in shaft vibration. One important reason for using reduced coefficients is the inability of most general purpose rotordynamic softwares to accept the full bearing matrix. It is hoped that the present study will add to the pool of knowledge regarding the pad motion tracking and frequency content.

The assumption about pivot friction and its' effect on bearing properties is addressed by researchers in the subsequent three papers.

Nicholas [3] is the first researcher to discuss the 'friction hypothesis' and how excessive friction between the pivot and the pad can impede pad motion. Impeded pad motion results in poor shaft tracking by the pads. He presented a simple model, shown in *Fig 4.3* to show the forces and moments involved in pad motion. Assuming point contact between the pivot and the pad, a load W_p on the pad produces a frictional force F_{fric} at the pivot. A dynamic force (due to unbalance, for example) F_n produces a

tilting moment M_n about the centre of the pivot, *'O'*. This moment can cause tilting of the pad only when it exceeds the frictional moment M_f that is resisting it.

or, the condition for pad motion can be expressed mathematically as follows:

$M_n > M_f$, where $M_f = F_{fric}.R_p$; $M_n = [F_{nx}.(R_p+L_2)] + (F_{ny}.L_1)$

Thus very large diameter pivots, though good from contact stress point of view are not acceptable from the pad motion perspective.

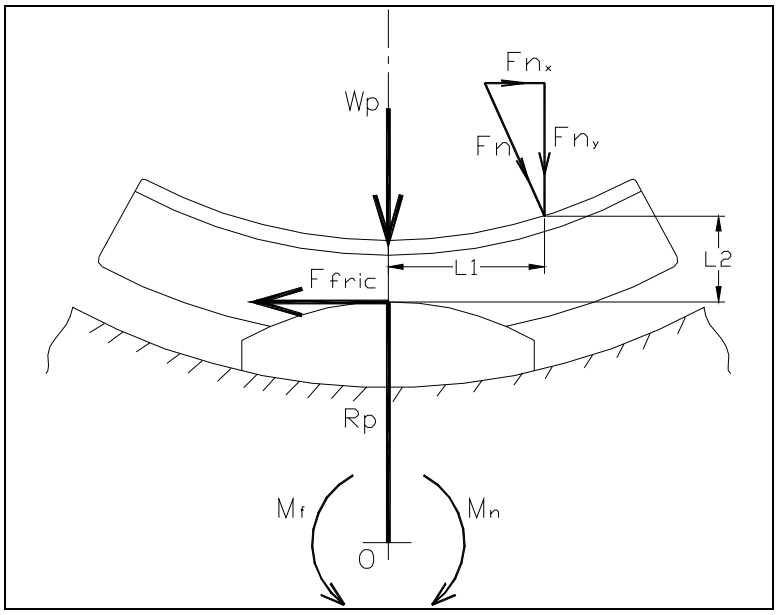

Fig 4.3 Dynamics of pad motion in a spherical pivot bearing (Ref [3])

Wygant et al. [13, 14] present the only available experimental work on the study of the influence of pivot friction on the static and dynamic properties of spherical pivot bearings. They compared the static (operating eccentricity, locus of journal equilibrium and oil film profile) for two identical tilting pad bearings. The only difference in the bearings was the type of pivots used. Line contact 'rocker back' pivot was used on one while seated ball in sphere was used in the other. Significant departure in the static behaviour was noted in the spherical pivot bearing and this was attributed to the increased friction.

Figures 4.4 and *4.5* show the locus of the shaft center for varying loads at three speeds (900, 1650 and 2250 rpm) for the rocker back and the SPB respectively.

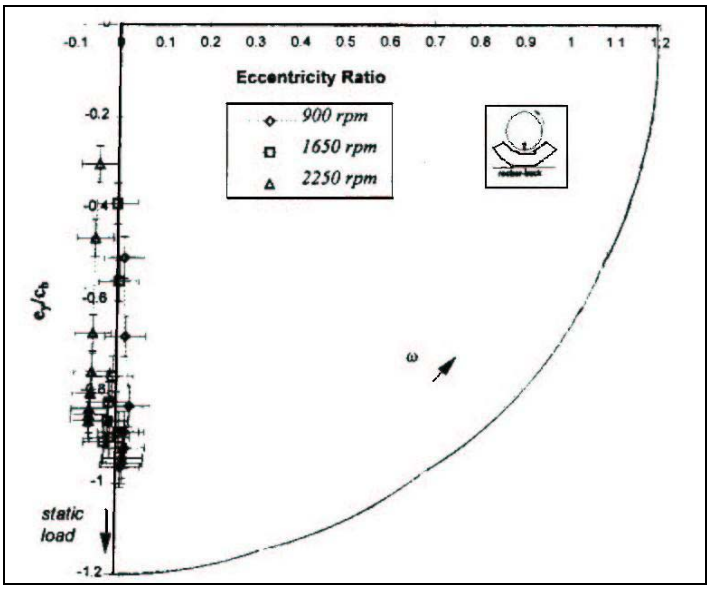

Fig 4.4 Shaft center locus for rocker back bearing (Ref [13])

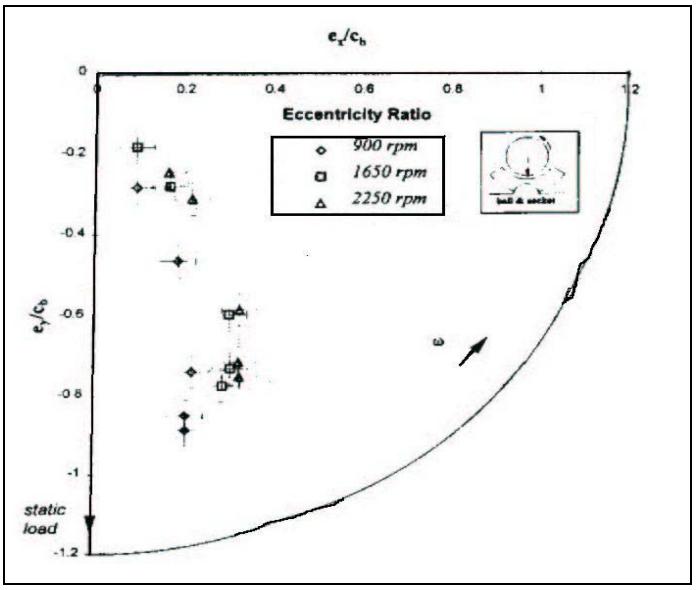

Fig 4.5 Shaft center locus for Spherical pivot bearing (Ref [13])

The near vertical locus for all speeds in case of the rocker back bearing proves almost complete absence of cross coupling forces. On the other hand, the strong semi-circular locus in case of the SPB indicates the presence of cross coupled forces. Such forces can be generated in a tilting pad bearing only when the pads do not adequately track the shaft.

As a direct extension to the above study, the authors also conducted comparison of the dynamic properties of the same set of bearings. Sinusoidal excitations were applied to the rotor-bearing system and the bearing dynamic characteristics were extracted. The

rocker back showed an almost complete absence of cross coupled stiffnesses while the other pivot configuration shows relatively high values of the forces. This again was attributed to the increased friction and lack of sufficient pad tracking. *Figures 4.6* and *4.7* show the non-dimensional cross coupled stiffness (K_{xy}) plotted vs. the Sommerfeld number for the rocker back and the SPB respectively.

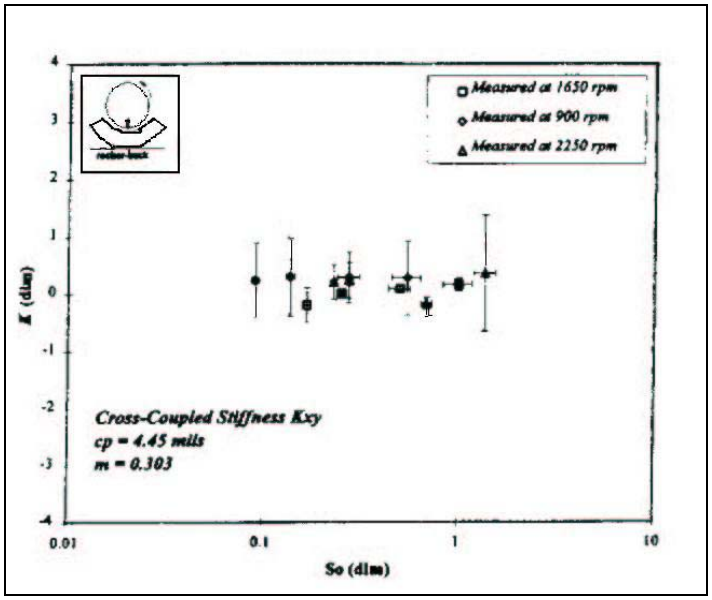

Fig 4.6 K_{xy} vs. *So* for the rocker back bearing (Ref [14])

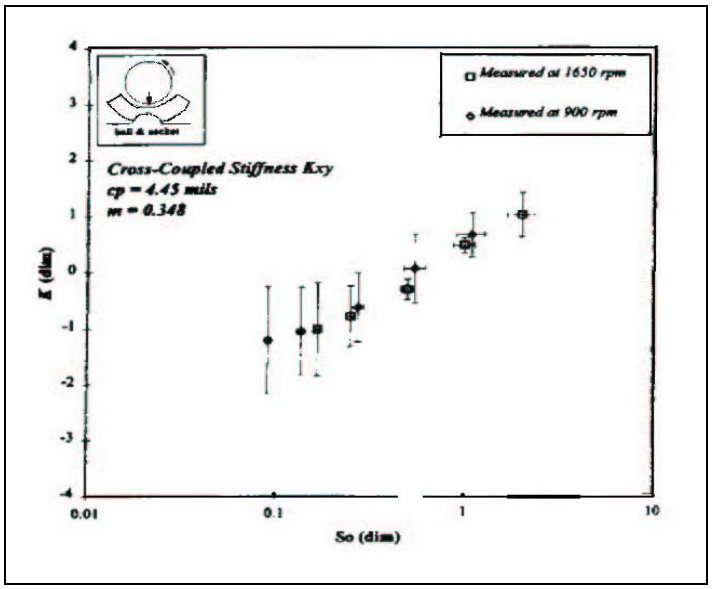

Fig 4.7 K_{xy} vs. *So* for the Spherical pivot bearing (Ref [14])

4.3 Current experiment strategy

Test procedure: Various sub-systems of the test rig previously mentioned are energized sequentially as per the startup procedure given in Appendix-I. Once the rig is operational, the rotor is started. After reaching the test speed it is allowed to operate "at speed" until steady oil/pad temperatures and shaft vibrations are achieved. A combination of a known unbalance and a steady load (horizontal, vertical or in any other direction) generated by the magnetic loading system is then applied on the rotating shaft and the vibrations of the shaft on either sides of the bearing are monitored. Simultaneously, the pad motion, also vis-à-vis the bearing housing, is monitored on either side. The shaft vibration probes are mounted at the same angle as the pad probes, albeit at different axial planes (1.25" from the inside and outside probes). See *Fig. 4.8* below for a schematic of the probe arrangement. The vibration data of all the instruments, that is, the 4 pad probes (from the two upper pads) and 4 corresponding shaft probes, is digitized and stored by the ADRE data acquisition system. This exercise is repeated for a number of combinations of rotor speed, magnetic load and unbalance. Each combination represents one test case. The test cases were so chosen as to cover the complete operating range of the bearing. The oil inlet temperature, pressure and rotor speed are held constant during the duration of the test.

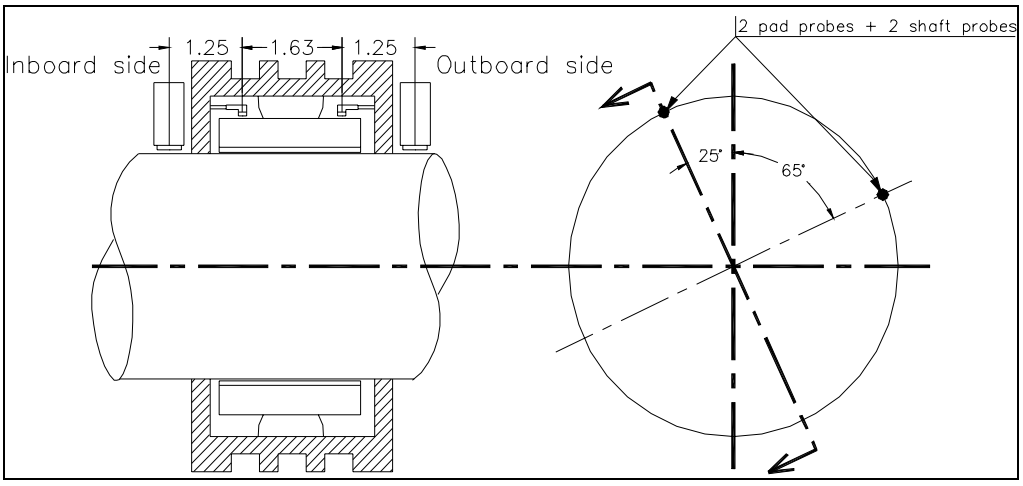

Fig 4.8 Arrangement of shaft and pad probes in the bearing

Qualitative comparison between shaft and pad motion: ADRE software from Bently Nevada was used for data acquisition and analysis. It has several excellent data presentation formats described in Section 3.3 which can be directly used in this study. The following strategy is applied for comparing the vibration signals from the pads and the shaft. The ultimate objective is to qualitatively assess the shaft tracking behavior of the pads.

1. Time trace waveform comparison: The synchronous filtered (1x) pad motion at any one probe is compared with the synchronous shaft vibration at the same angle. The keyphasor mark acts as a reference and a simple visual comparison is made between the two. The parameters of interest are the position of peak with respect to keyphasor mark, ratio of peak-to-peak amplitudes and the variation of this ratio with shaft speed and unbalance.
2. Frequency components comparison: For various test cases, a comparison is made between the shaft and pad motion signals in the frequency domain. The popular 'Half" spectrum plots supported by ADRE are used for this purpose. Since orthogonal probe pairs are not used, a full spectrum (showing the forward and backward components separately) cannot be used. However, it is possible to verify what frequency components are present in each signal. This would also reveal the proportion of the shaft synchronous component and other frequency components in the pad motion.

Chapter 5 presents a summary of the various test cases and the data collected for each case. The data is then analyzed and how it stands with respect to the two assumptions is separately addressed.

Chapter 5

Test results and Analysis

The results for the various test cases are presented in this chapter together with the analysis of the data. The test cases are first summarized and then the results relevant to each of the two assumptions under investigation are presented and analyzed separately.

5.1 Summary of test results

The test cases are summarized and tabulated below. They cover a wide range of operations of the bearing and hence the present study can be considered to be representative of the behavior of the bearing under most field conditions. The dimensionless Sommerfeld number is used as the basis of comparison. It is calculated as follows:

$$So = \left(\frac{\mu NDL}{60.W}\right) * \left(\frac{R}{c}\right)^2,$$

Where, μ = viscosity of the oil (reyns), An average of 94° F has been considered and $|\text{viscosity}|_{94^\circ F} = 4.826 \times 10^{-06}$ reyns; N = rotor speed (rpm); D = bearing diameter (in); L = Pad length (in); R = bearing radius (in); c = Assembled bearing radial clearance (in); and, W = load on bearing (lb);

'W' is computed from the load indicated by the load cells under the magnetic loading system and not from the load cells under the bearing for reasons mentioned earlier. Let M = Magnitude of load exerted by magnet assembly on rotor (lb), then $W = \overline{(0.774 * M)} + \overline{75}$, in other words, it is the vector sum of the rotor static weight on the test bearing (75 lbs) and the portion of load transferred to the test bearing by the magnets. The various test cases are shown in Table 5.1. Henceforth, 0° is vertically up, 90° is horizontal to the left looking into the bearing, 180° is downwards and 270° is to the right hand side.

Table 5.1 Experimental test conditions

Speed (rpm)	Load on rotor due to magnets (M)		Load on bearing (W)		So (dim)
	Mag. kg (lb)	Angle	Mag. kg (lb)	Angle	
4000	680.4 (1500)	180°	561 (1236)	180°	0.728
4000*	**680.0 (1500)**	**48°**	**502 (1106)**	**45°**	**0.814**
6000	680.4 (1500)	180°	561 (1236)	180°	1.093
7000	544.3 (1200)	0°	387 (853.8)	0°	1.846
6000	453.6 (1000)	0°	317 (699)	0°	1.933
5000	226.8 (500)	180°	209 (462)	180°	2.437
4000	226.8 (500)	0°	141 (312)	0°	2.887
4000	181.4 (400)	0°	106 (234.6)	0°	3.839
4000	90.7 (200)	180°	104 (230)	180°	3.916
5000	181.4 (400)	0°	106.5 (234.6)	0°	4.799
4000	136.1 (300)	0°	71.4 (157.2)	0°	5.730
6000	181.4 (400)	0°	106.5 (234.6)	0°	5.759
7000	90.7 (200)	0°	36.2 (79.8)	0°	19.754
5000	27.2 (60)	0°	13.0 (28.56)	180°	39.420

***Load on pivot case**

Range of Sommerfeld number studied by Wygant et al. [13, 14]: 0.1~2.0

It can be seen that a wider range of Sommerfeld number has been covered by the present study in comparison to the study by Wygant et al. [13, 14].

5.2 Pad motion frequency studies

The first part of the experiment was aimed at verifying the pad motion frequency. As explained in Section 3.3, the FFT of the vibration signals of the shaft and a pad were compared and the results so obtained are tabulated and presented in Table 5.2. It can be clearly seen from the table that a pad has all the frequency components that the shaft has and none besides. In other words, there are no frequency components in the pad plots that are not present in the shaft plots and vice-versa. This validates the use of synchronously reduced bearing coefficients when the shaft is executing predominantly synchronous vibrations.

Table 5.2 Frequency components in shaft and pad vibrations

So	Shaft/Pad 1x frequency (CPM)	Additional components in shaft spectrum	Additional components present in pad spectrum
0.728	4000	2x	2x
0.814	4000	1.37x*, 2x, Low noise	1.37x*, 2x, Low noise
1.093	6000	None	None
1.846	7000	None	None
1.933	6000	None	None
2.437	5000	Low noise	Low noise
2.887	4000	Low noise, 2x	Low noise, 2x
3.839	4000	Low noise, 2x	Low noise, 2x
3.916	4000	1.41x*, 2x, noise	1.41x*, 2x, noise
4.799	5000	1.42x*, 2x, noise	1.42x*, 2x, noise
5.730	4000	Low noise, 2x	Low noise, 2x
5.759	6000	None	None
19.754	7000	None	None
39.420	5000	2x	2x

* Unexplained super-synchronous components present in the vibration signal

The 'low noise' mentioned in the table refers to very low amplitude (<0.01 mils) components of random frequencies present in the spectrum. They are due to the extremely small amplitudes of observed motion and random noise in the signal.

From the above table, all the test cases with little or no noise are selected and further analyzed. The ratio of amplitudes of various components of the signals (shaft and pad) are calculated and tabulated below in Table 5.3.

Table 5.3 Amplitude comparison for shaft and pad vibrations

So (dim)	(shaft/pad) direct peak-peak	(shaft/pad) 1x peak-peak	(shaft/pad) 2x peak-peak	Location from TDC
0.728	2.486	4.12	7.31	Left pad
1.093	2.866	2.885	--	Left pad
1.846	2.567	3.520	--	Left pad
1.933	2.423	3.970	--	Left pad
5.759	3.258	5.242	--	Left pad
19.754	3.842	5.826	--	Left pad

From Table 5.3, it can be clearly seen that the ratio of direct shaft motion to direct pad motion is roughly in the range of 2.5 to 4.0.

This ratio varies with the Sommerfeld number in a somewhat erratic manner but it can be seen that the ratio generally increases as the load on the bearing decreases.

Over the next four figures, the half spectrum (FFT) plots of one of the instrumented pads together with the corresponding shaft probes are shown. They show the FFT plots from the outboard and inboard probes on one of the two pads in the top half while the corresponding shaft plots are in the bottom half. Plots shown in *Fig 5.1* are at the highest loading (*So* = 0.728) and the 1x component can be clearly seen in both the shaft and pad spectrum plots. Also a small 2x component is visible in all the plots.

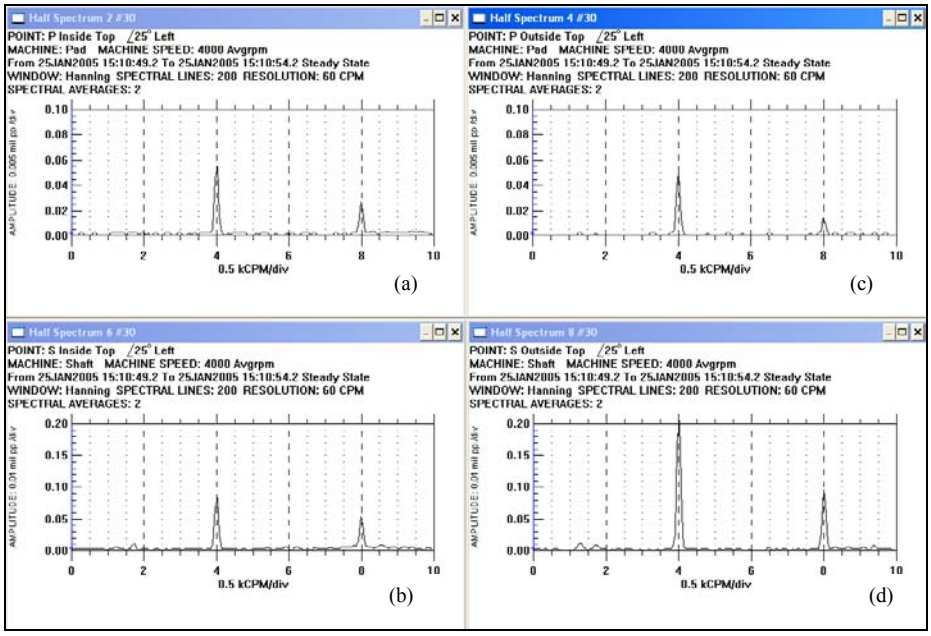

(a) Top pad inside
(b) Top shaft inside
(c) Top pad outside
(d) Top shaft outside

Fig 5.1 FFT plots (*So* = 0.728, *N* = 4000 rpm)

Figure 5.2 shows the spectrum plots for the lone load on pivot case, here too the frequency content of the shaft vibrations and corresponding pad motions are identical.

The shaft vibrations had a mysterious component (~ 1.4x) reported earlier attributed either to structural vibration or belt flapping. Regardless of the origin of this component, it was faithfully present in the pad motion too. Also visible is the noise floor on all the channels.

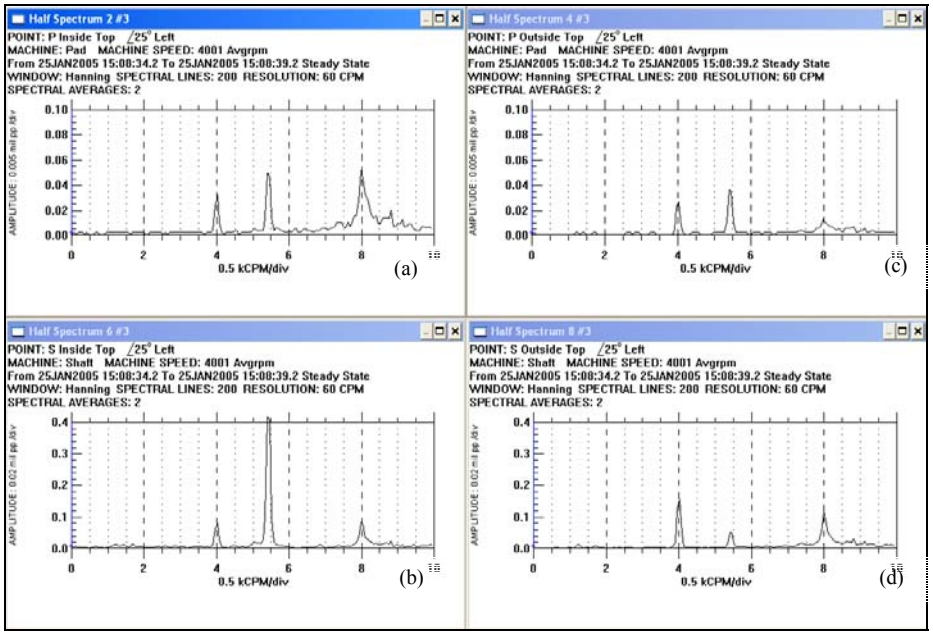

(a) Top pad inside
(b) Top shaft inside
(c) Top pad outside
(d) Top shaft outside

Fig 5.2 FFT plots (*So* = 0.814, N = 4000 rpm, load on pivot case)

Fig 5.3 shows the component comparison for the highest speed case (7000 rpm).

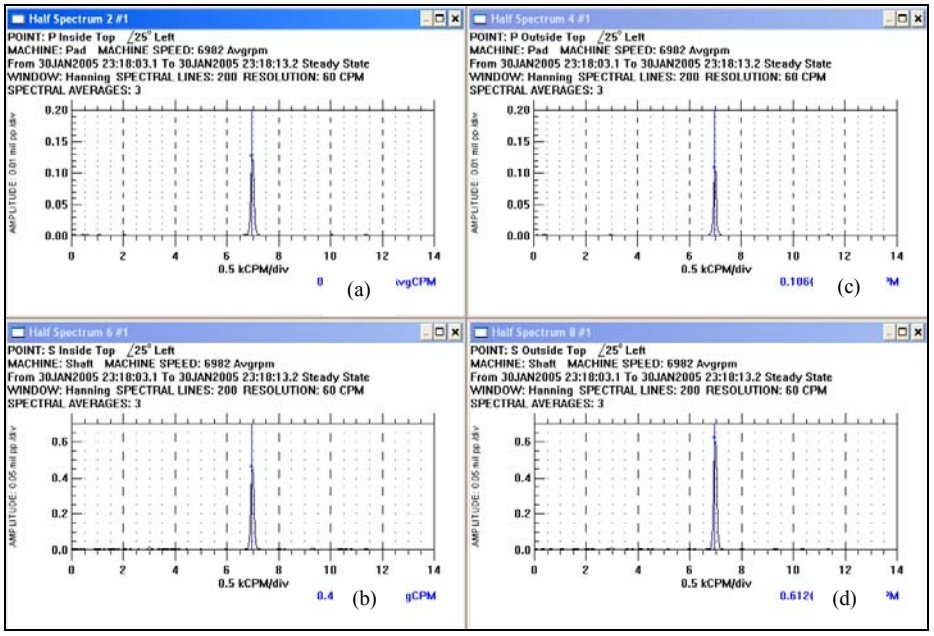

(a) Top pad inside
(b) Top shaft inside
(c) Top pad outside
(d) Top shaft outside

Fig 5.3 FFT plots (*So* = 19.754, *N* = 7000 rpm)

Figure 5.4 below shows the case with the lowest loading (*So* = 39.42). In this case too there is a large 1x component in all the FFT plots together with a small 2x component (10,000 CPM). Both the components are present in both the shaft and the pad vibrations.

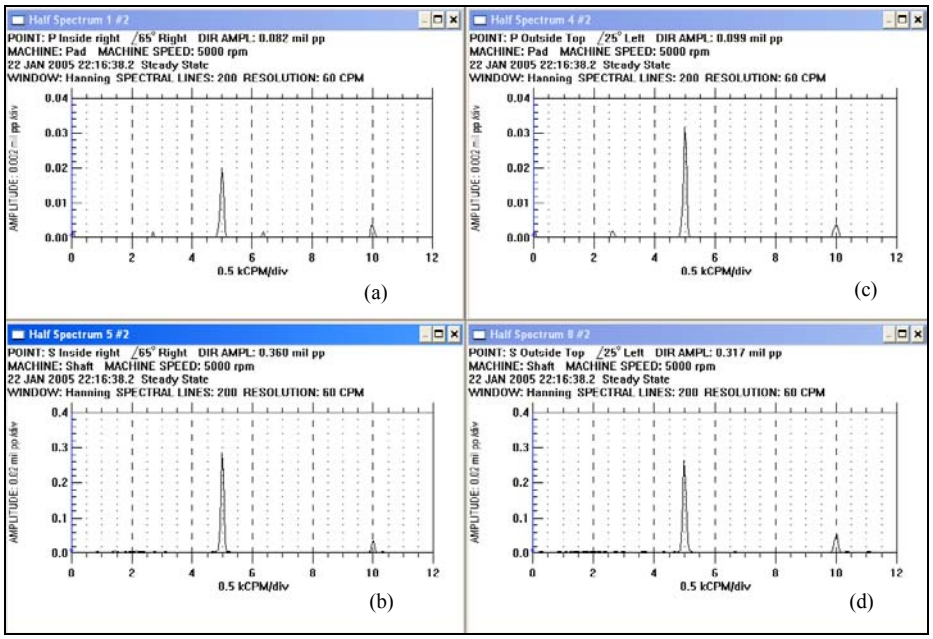

(a) Right pad inside
(b) Right shaft inside
(c) Right pad outside
(d) Right shaft outside

Fig 5.4 FFT plots (*So* = 39.42, *N* = 5000 rpm)

5.3 Shaft tracking behavior studies

To verify the shaft tracking characteristic of the pads, the following strategy was adopted. The 1x filtered time trace of a pad probe and the corresponding shaft probe was compared for the phase difference between the two. The keyphasor mark was used as the reference. The results are tabulated below in Table 5.4.

Table 5.4 Phase comparison for shaft and pad vibrations

So (dim)	Shaft speed (RPM)	Inside		Outside	
		Phase difference	ADRE plot #	Phase difference	ADRE plot #
0.728	4000	1° lead	450 L	37° lead	450 L
0.814	4000	127° lead	13 L	11° lead	13 L
1.093	6000	3° Lag	690 R	30° lead	690 R
1.846	7000	128° lead	178 L	20° lead	178 L
2.437	5000	142° Lag	13 L	56° lead	13 L
2.887	4000	102° lead	5 L	36° lead	5 L
3.839	4000	102° lead	3 L	34° lead	3 L
5.759	6000	114° lead	3 L	24° lead	3 L
19.754	7000	138° lead	12 L	16 ° lead	12 L
39.420	5000	104° lead	4 L	25° lead	4 L

A note on phase determination

Keyphasors are the preferred instruments for determining the phase angle in vibration measurement. *Figure 5.5* below shows how the phase in reckoned for an example case. The phase angle (Φ) is defined as the ratio of the time from the keyphasor mark to the next positive peak (t) to the time period of the signal (T) expressed in angle units.

$$\phi = 2\pi\left(\frac{t}{T}\right)$$

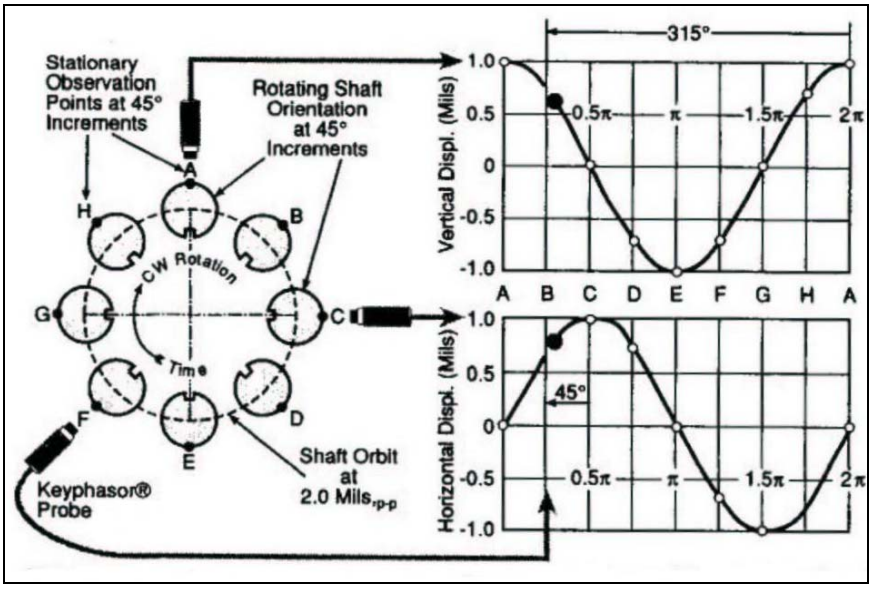

Fig 5.5 Phase determination using keyphasor (Ref [1])

Phase difference between the pad and shaft vibration signals is calculated by subtracting the phase angle of the pad signal from the phase angle of the shaft signal. The unexpected and surprising fact to be noted here is that the pad motion LEADS the shaft motion in most cases. *Figure 5.6* shows the highest '*So'* case while *Fig 5.7* shows the next highest '*So'* case.

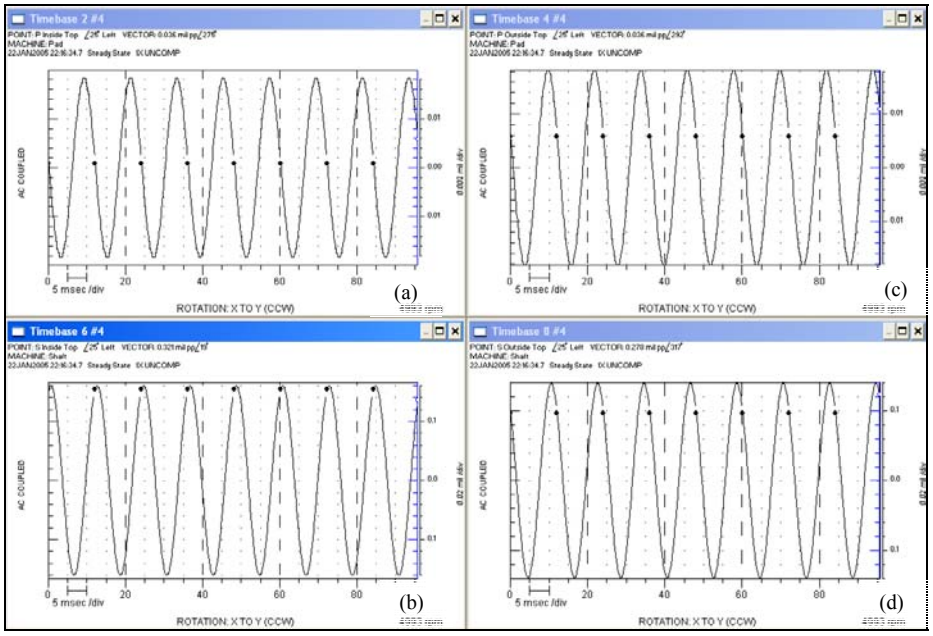

(a) Top pad inside
(b) Top shaft inside
(c) Top pad outside
(d) Top shaft outside

Fig 5.6 Time trace comparison (*So* = 39.420 case)

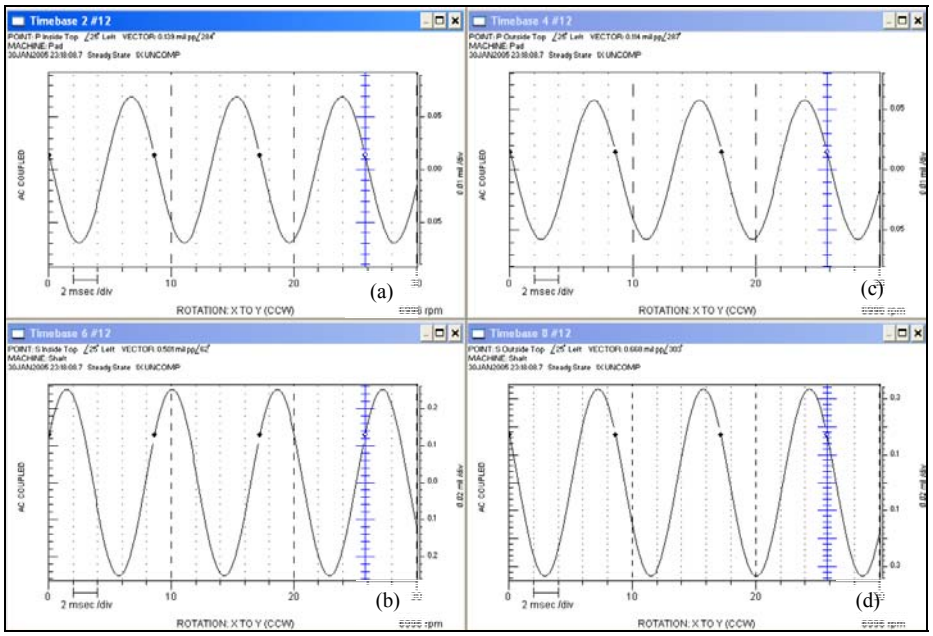

(a) Top pad inside
(b) Top shaft inside
(c) Top pad outside
(d) Top shaft outside

Fig 5.7 Time trace comparison (*So* = 19.754 case)

Figure 5.8 below shows the *So* = 5.759 case while *Fig 5.9* shows the *So* = 3.839 case. The *So* = 2.887 case is shown in *Fig 5.10*

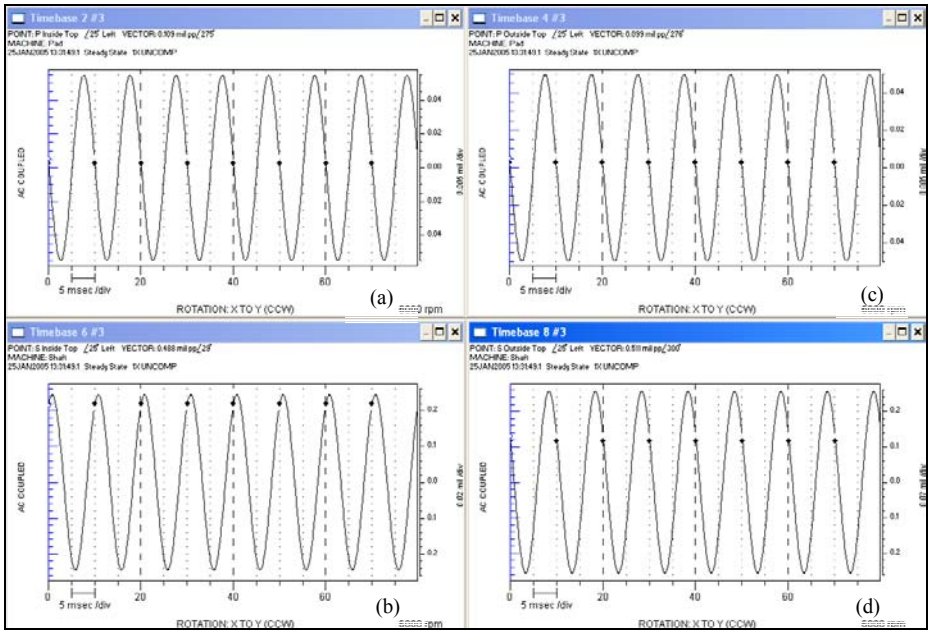

(a) Top pad inside
(b) Top shaft inside
(c) Top pad outside
(d) Top shaft outside

Fig 5.8 Time trace comparison (*So* = 5.759 case)

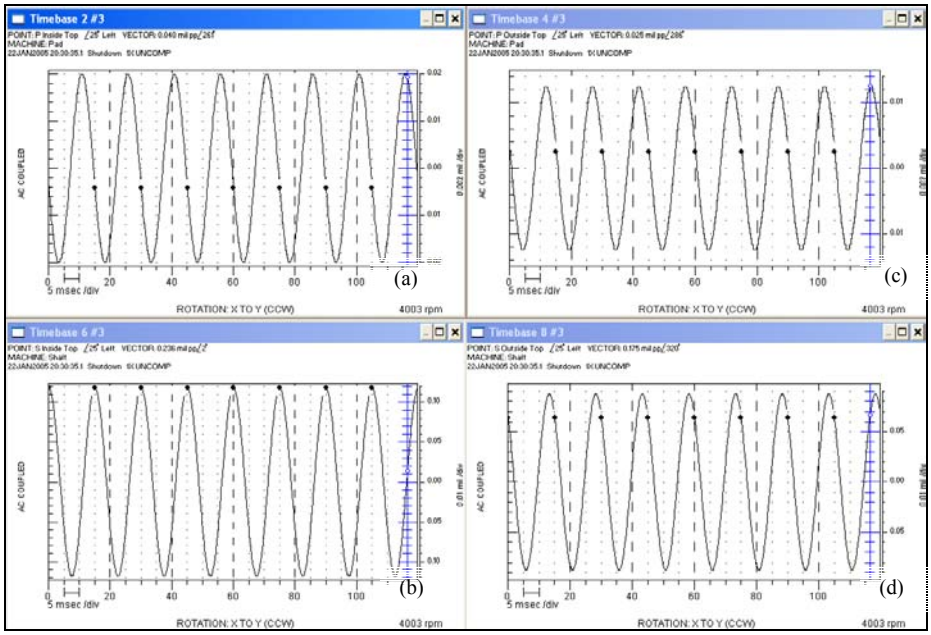

(a) Top pad inside
(b) Top shaft inside
(c) Top pad outside
(d) Top shaft outside

Fig 5.9 Time trace comparison (*So* = 3.839 case)

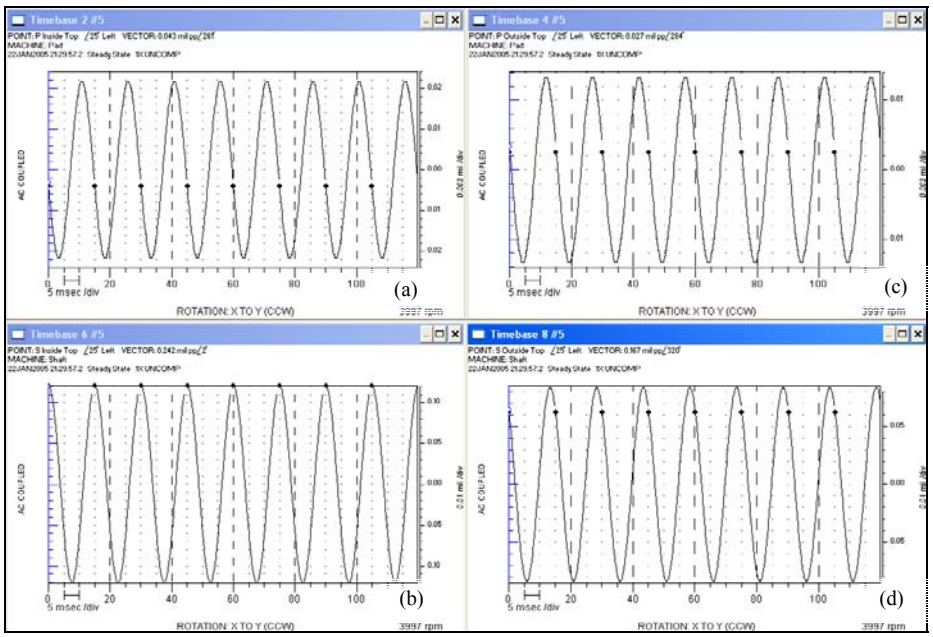

(a) Top pad inside
(b) Top shaft inside
(c) Top pad outside
(d) Top shaft outside

Fig 5.10 Time trace comparison (*So* = 2.887 case)

The following figure (*Fig. 5.11*) shows one of the few cases where the pad motion LAGS the shaft motion. This happens at only two values of the Sommerfeld number, the figure below shows the *So* = 2.437 case.

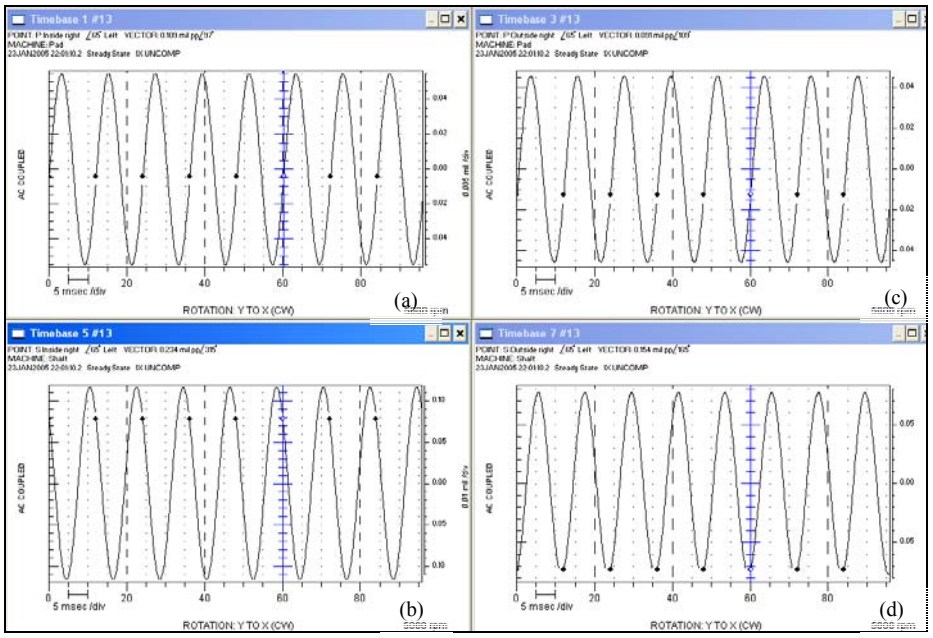

(a) Top pad inside
(b) Top shaft inside
(c) Top pad outside
(d) Top shaft outside

Fig 5.11 Time trace comparison (*So* = 2.437 case)

Figure 5.15 depicts the highest loading situation. The pad motion leads the shaft motion as seems to be the normal trend. This is also the case in the only 'load on pivot' case shown in *Fig 5.14*.

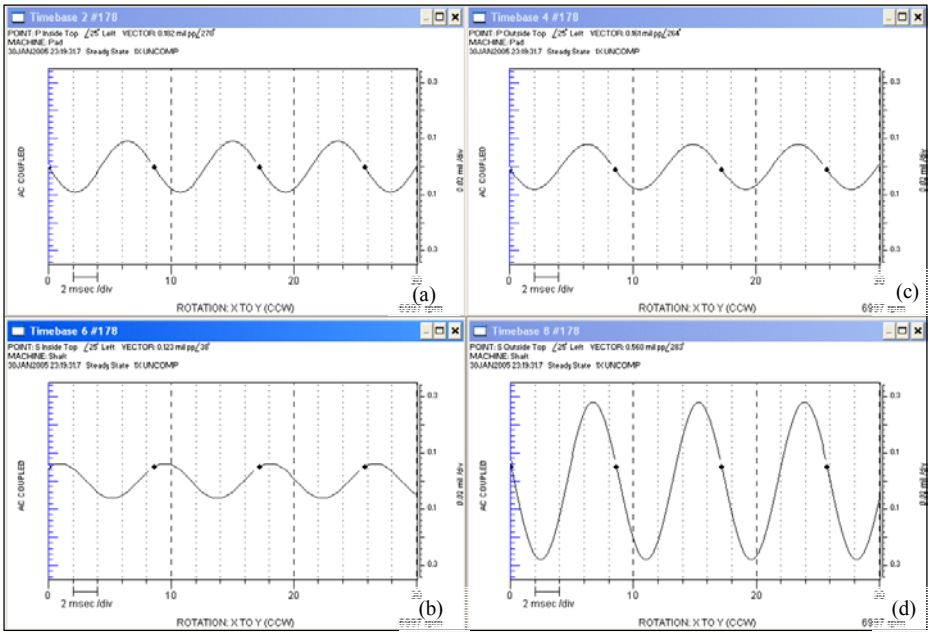

(a) Top pad inside
(b) Top shaft inside
(c) Top pad outside
(d) Top shaft outside

Fig 5.12 Time trace comparison (*So* = 1.846 case)

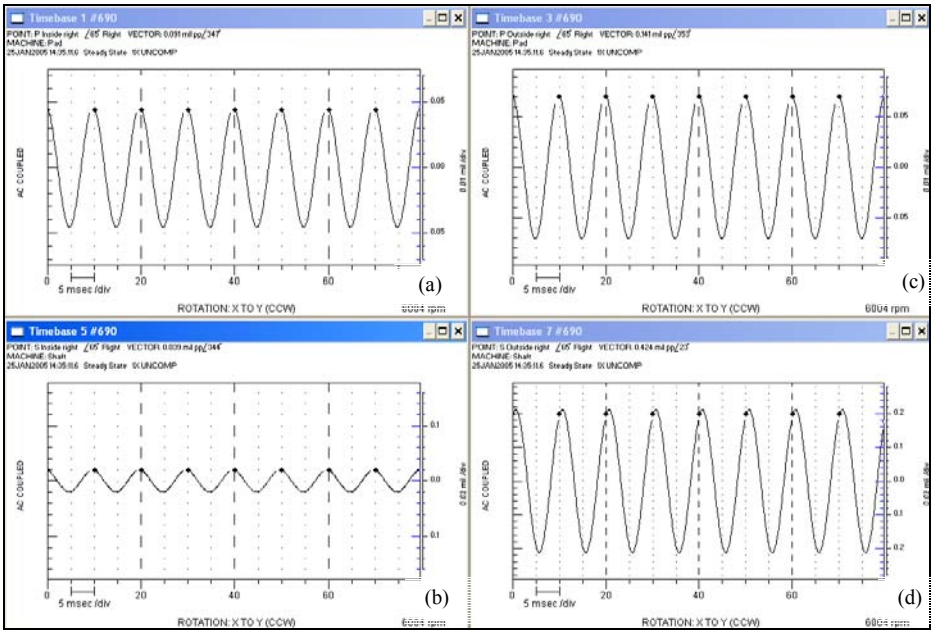

(a) Right pad inside
(b) Right shaft inside
(c) Right pad outside
(d) Right shaft outside

Fig 5.13 Time trace comparison (*So* = 1.093 case)

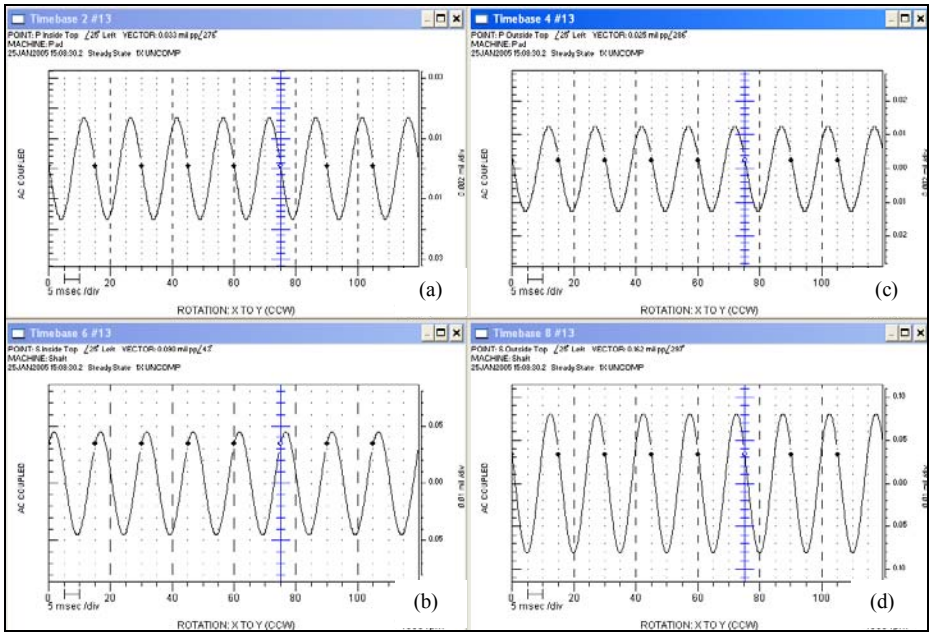

(a) Top pad inside
(b) Top shaft inside
(c) Top pad outside
(d) Top shaft outside

Fig 5.14 Time trace comparison (*So* = 0.814 case)

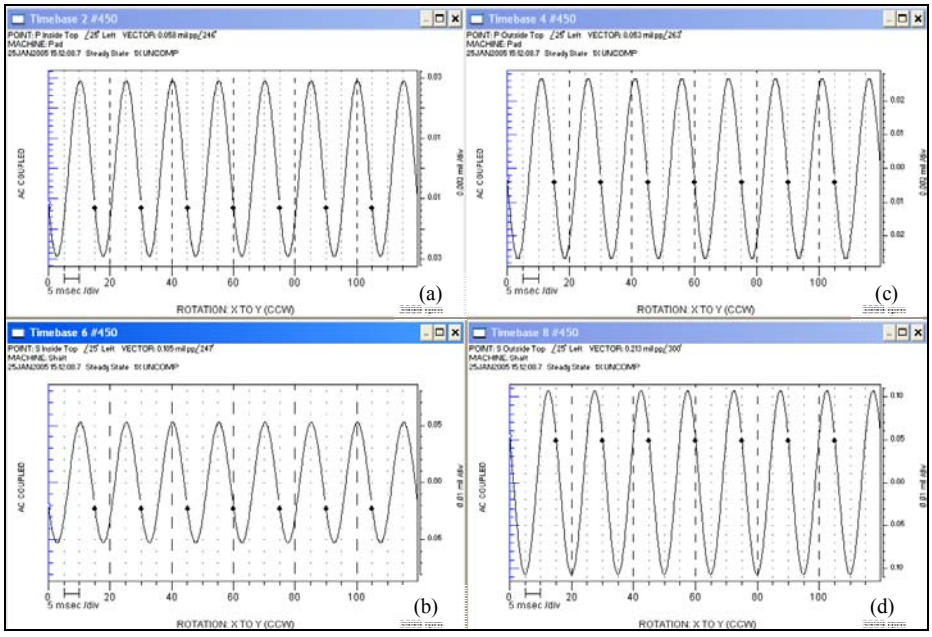

(a) Top pad inside
(b) Top shaft inside
(c) Top pad outside
(d) Top shaft outside

Fig 5.15 Time trace comparison (*So* = 0.728 case)

Chapter 6

Conclusions and Recommendations

The material presented in this thesis concludes with this chapter. The first part of the chapter brings out the conclusions drawn from the data collected and analyzed in the previous chapter. It has to be mentioned at this juncture that the conclusions are only preliminary in nature. There is scope for more exhaustive experimentation and analysis in this area. Some recommendations for future experimentation and investigation are made in the second part of this chapter. It is hoped that they are a good starting point for future researchers interested in the field of pad motion.

6.1 Conclusions

The following conclusions can be drawn from the analysis presented in the earlier chapter.

1. This study of pad motion frequency has clearly demonstrated that all the frequencies present in the shaft can be observed in the pad motion too. This happens at all values of the Sommerfeld number covered in the experiment.
2. The ratio of the amplitudes of the different components in the shaft motion to the corresponding ones in the pad motion is approximately the same.
3. The previous conclusions support the use of synchronous coefficients for forced response and stability calculations for conditions with dominant synchronous content in shaft vibration. But in case non-synchronous excitation is dominant, it then would be correct to use bearing coefficients of corresponding frequency.
4. In spite of the fact that spherical pivot bearings are self-aligning, the pad surface is not exactly parallel to the shaft at all times. There is a perceivable amount of angular misalignment from the inside of the pad to the outside with respect to the shaft.

5. As far as shaft tracking by the pads is concerned, the pad motion leads the shaft motion. The amount of lead varies with the Sommerfeld number and does not seem to follow a fixed pattern. Further experimentation is necessary to fully understand the shaft tracking behavior.

6.2 Recommendations

The experience gained in the current study can be used by future researchers in this area and can help them overcome problems encountered and also look into aspects not covered in the present study. The following recommendations are made:

A true measure of the shaft tracking behavior of SPBs is possible only if their performance is compared to that of the more traditional bearing configurations (rocker back, sphere on cylinder etc.). Hence it is recommended that identical tests be conducted on a SPB and at least another bearing, identical in all respects except the pivot types and a full comparison made.

The effect of manufacturing variables like the pivot roughness, the clearance between the ball and the cavity and material of pivot and pad etc. can be investigated to obtain a better understanding of the behavior of SPBs in the field.

A better and more mathematical measure of correlation of the pad and shaft motion has to be developed.

Tests at higher speeds have to be carried out to study the high frequency response of the pads. The onset of pad flutter in the unloaded can be directly investigated.

Non-synchronous excitation can be applied to the shaft and the behavior of the pads can be investigated to see what happens during various aero-dynamic instabilities of the rotor.

As far as the existing FFJB test rig is concerned, better instrumentation and data acquisition can be used to eliminate noise and to achieve better resolution.

References

1. Eisenmann R C and Eisenmann R C Jr. “Machinery malfunction: Diagnostics and correction”, Prentice hall, 1998, ISBN: 0-13-240946-1
2. Kirk, R G. Reedy, S W. “Evaluation of Pivot Stiffness for Typical Tilting-Pad Journal Bearing Designs” [Journal Article] Journal of Vibration & Acoustics-Transactions of the ASME. v 110 n 2 Apr 1988 p 165-171
3. Nicholas, J C. Wygant K D. “Tilting Pad Journal Bearing Pivot Design for High Load Applications”, Turbo Symposium, Texas A & M University, 1995
4. Nicholas, J C. “Tilting Pad Journal Bearings with Spray-Bar Blockers and Bypass Cooling for High Speed, High Load Applications”, Turbo Symposium, Texas A & M University, 2003
5. Nicholas, J C.; Gunter, E J.; Allaire, P E.; “Stiffness and Damping Coefficients for the Five-Pad Tilting-Pad Bearing” Tribology Transactions. v 22, n 2, Apr 1979 p 113-124
6. Nicholas, John C. “Lund's tilting pad journal bearing pad assembly method” [Journal Article] Journal of Vibration & Acoustics-Transactions of the ASME. v 125, n 4, October 2003. p 448-454
7. Swanson, E E. and Kirk, R G. “Experimental temperature and pressure profiles for two steadily loaded journal bearings” [Journal Article] Tribology Transactions. v 38 n 3 Jul 1995. p 601-606
8. Swanson, E E. Kirk, R G. Mondy, R E. “Examination and comparison of the maximum film temperature in a journal bearing for 13 synthetic, mineral, and viscosity index enhanced oils”. [Conference Paper] SAE Special Publications. Publ by SAE, Warrendale, PA, USA, 922343. n 936. p 137-145
9. Swanson, E E. Kirk, R G. “Survey of experimental data for fixed geometry hydrodynamic journal bearings” [Conference Paper] American Society of Mechanical Engineers (Paper) 1996. ASME, New York, NY, USA.. 7p
10. Swanson; E E. Kirk, R G. “Bearing test rig dynamics problem identification and model tuning” [Journal Article] Shock & Vibration Digest. v 32 n 1 Jan 2000. p 39
11. Swanson; E E. “Evaluation of the VPI&SU fluid film test rig”, 1992, MS thesis, Virginia Tech
12. Swanson; E E. “Design and evaluation of an automated experimental test rig for determination of the dynamic characteristics of fluid film bearings”, 1998, PhD Thesis, Virginia Tech
13. Wygant, K D. Flack, R D. Barrett; L E. “Influence of pad pivot friction on tilting-pad journal bearing measurements - Part I: Steady operating position” [Journal Article] Tribology Transactions. v 42, n 1, Jan 1999. p 210-215
14. Wygant, K D.; Barrett, L E.; Flack, R D.; “Influence of pad pivot friction on tilting-pad journal bearing measurements- Part II: Dynamic coefficients” [Journal Article] Tribology Transactions. v 42, n 1, Jan 1999. p 250-256

Appendix

Operating Instructions

Virginia Tech Fluid film bearing test rig

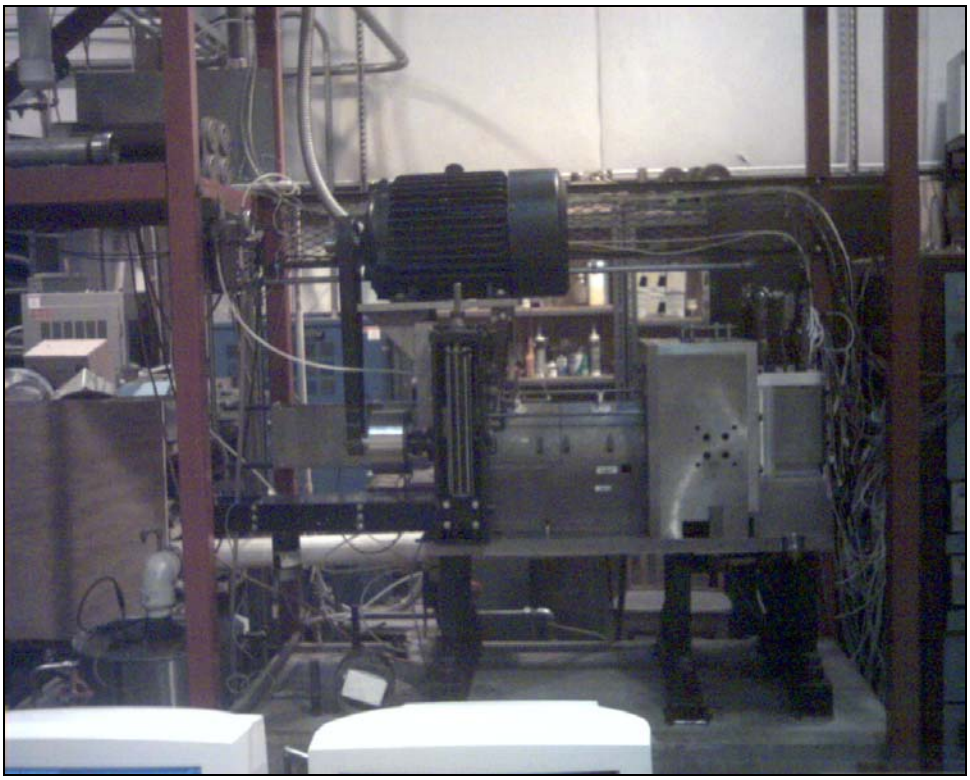

Prepared by: Giridhar Sabnavis

Approved by: Dr. R G Kirk

Rotor dynamics laboratory

Plantation Road Research Compound

Virginia Polytechnic Institute & State University

1. Turn on big air compressor (fig. 1) and let it run till local gage reads 120 psig. This should supply enough air for about an hour of rig operation. The air goes to the receivers outside the laboratory, which need to be periodically drained to remove any water collected. The air is necessary for the rear bearing oil mist and to operate the pneumatic valve. Open air valves near motor breaker panel and mist valve (fig. 2 & 3). Manual valves are open when the lever is in line with the piping.

Fig. 1 Big air compressor

Fig. 2 Control air manual valve & transmitter

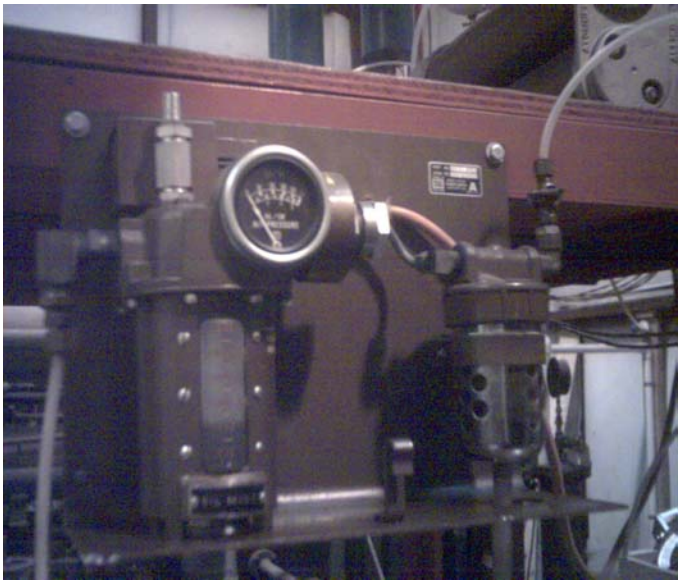

Fig. 3 Rear bearing oil mister

2. Turn on main valve for water (fig. 4). The gage should show a pressure of approximately 100 psig. Turn on manual valve near rig (fig. 5) to admit water into oil cooler through pneumatic control valve.

Fig. 4 Main valve with gauge

Fig. 5 Manual and Pneumatic valves

3. Switch on motor breaker (fig. 6).

Fig. 6 Motor breaker

4. Switch on 'MASTER POWER' on control panel (fig. 7). All the subsequent instructions are to be carried out from the control panel.
5. Turn on the oil pump motor (fig. 7) after opening pump isolation valves (fig. 8). Adjust relief valve near test bearing (fig. 9) till oil inlet pressure (as indicated by the local pressure gage on the rig) is approximately 10~15 psig (~4 gpm).
6. Switch on oil tank heater (fig. 7) and leave it turned on till oil temperature is approximately 100 °F (could take up to 15 mins. depending on the initial temperature of the oil).
7. The oil temperature controller (Yokogawa, see Fig. 7) should automatically open the Pneumatic valve (fig. 5) and the temperature is maintained at 100 °F. The oil heater can now be turned off.
8. Turn on 'COMPUTER/INSTR. POWER' on panel (fig. 7). This should turn on the computers, the oscilloscope, the oil temperature monitor and controller and rear bearing positioner

Fig. 7 Power control module

Fig. 8 Oil pump with isolation valves

Fig. 9 Pressure regulating valve

9. *Never turn on PWM power on without oil in the bearing. The magnets go unstable and result in the chatter of the shaft.*

10. The rear bearing can be aligned in any desired manner using the right-left and up-down movement controls. Alternately, the bearing can be automatically centered using the centering buttons (fig. 10).

11. Type 'WIN' to start MS-windows on both the computers.

12. On the left computer (when facing the panel), open the 'RIG CONTR' program. On the right computer, open the 'DAQTEST' program.

13. Switch on the 'PWM amplifier power' (Fig. 7) when the program prompts.

14. The 'RIG CONTR' program opens default in the 'DISP.' Mode, i.e. the position/displacement of the journal center can be set.

Fig 10 Rear bearing positioner

15. Switch on the "MOTOR DRIVE POWER" on the panel.

16. To run the rig manually, enter a speed (less than 6000 rpm) and click on 'START'. To modify the force applied on the rotor by magnets, bring the control to 'FORCE' mode and input a new load and orientation (-90° is vertically downward).

17. While in the 'FORCE' control mode, if the 'Force prop. Gain' is set too low, it takes relatively longer time to reach the set load, while too high a value makes the system hunt and never stabilize (typical value: 0.2) Ditto with 'Disp. Prop gain' and 'Speed prop. Gain' (typical values: $1e^{-5}$ and $4e^{-3}$ respectively)

18. The forces transmitted on the four load cells under the test bearing are shown in the right computer under the following names: "IB LLd, IB RLd, OB LLd, OB RLd (Analog channels 8 – 11)".

19. The scope shows the shaft orbit if the 'X' and 'Y' channels are connected any orthogonal set of probes. (Usually connected to Inside left and Inside bottom probes).

20. To run an automatic test case, open 'MATLAB' on the right computer. Open any stest*.m file, copy it and rename file as required. Make suitable modifications (as explained below) and run the file.

21. For completely shutting down the system from this point, one has to basically follow the reverse sequence of events

22. Turn off the PWM amplifier and motor power, close all programs and then MS-windows on both computers.

23. Turn off 'COMPUTER/INSTR. POWER'. Leave oil pump running for 10 more mins. Then turn off oil pump and 'MASTER POWER'.

24. Close air supply to oil mist (fig. 3), close manual water valve (fig. 5) and ensure that main water valve is closed (fig. 4). To obtain correct value of line pressure, crack open the little valve connected to the gauge to release pressure. Close motor breaker (fig. 6).

"stest.m" runs steady state test on the bearing with different loads at a fixed speed*

Enter loads ('x 'and 'y') and speed (rpm) into the code as shown below:

```
loads = [0 -400
         0  400
         400  0
        -400 0];
rpm = 3000;
```

The program then initializes the data acquisition system etc. and draws four plots

a. Averaged x vs. y
b. x and y vs. load
c. brg. T/c temp vs. load
d. orbit

The program prompts the user to set the journal at any desired position (using the rear bearing positioner) and then press 'ENTER'

```
disp('set pos, hit enter');
pause
poss = pzdata;
```

After every load step, the program pauses for some time (toc) for the system and readings to stabilize and then collects data. Before going to the next load set, it return the shaft to the set location.

```
% start timer
  tic;
  while (toc < 10)
```

After all the load cases are run, the program saves all the data collected during the test (xpos, ypos, speed, load, brg. Temp etc.) and shuts down the system. The data (variables) can be transferred to MS-excel for further analysis.

Contents of panel

1. Top most drawer:
   - 18 channels for 'K' type thermocouples for bearing outer housing
   - 18 channels for 'J' type thermocouples for bearing metal
   - 14 channels for pressure gauges
   - Power supplies for above and digital Oil tank temperature indicator (°C)
2. Next from top:
   - 10 nos. Bently proximity probe drivers (8x3300/8mm + 2x7200/5mm)
   - 2 nos. Magnet load cell signal conditioning cards
   - 4 nos. Bearing load cell signal conditioning modules
3. Left computer (rig control) CPU
4. Right computer (data acquisition) CPU
5. A/D and D/A converters
6. Bottom most rack:
   - 3 nos. PWM amplifiers
   - Power supply

Vita

Giridhar Sabnavis was born on the 8th of March, 1976 in India. After graduating from high school in 1993, he earned his BS in Mechanical Engineering in 1997. It was during that time that he developed a passion for turbomachines. On graduation he joined BHEL, a leading manufacturer of industrial and power equipment in early 1998. He spent the next five years in the turbocompressor design department where he was responsible for the successful and timely design, manufacture and commissioning of several high speed centrifugal compressors. He also spent some time in the turbocompressors and steam turbines technical proposals group. He was responsible for making successful bids for at least two prestigious and high value compressor packages. In 2002 he came to VPI & SU for pursuing graduate studies in the Mechanical Engineering department. He was a graduate researcher in Dr. Kirk's Rotordynamics laboratory and helped organize several technical meetings and conducted several experimental studies on tilting pad bearings. He hopes to gain employment in a turbomachinery engineering company and apply his knowledge in rotordynamics and design towards practical realization.